JOC Article

Synthesis, Electrochemical, and Optical Properties of Linear Homo- and Heterometallocene Triads†

Antonio Caballero, Arturo Espinosa, Alberto Tárraga,* and Pedro Molina*

Departamento de Química Orgánica, Facultad de Química, Universidad de Murcia, Campus de Espinardo, E-30100 Murcia, Spain

pmolina@um.es; atarraga@um.es

Received May 26, 2007

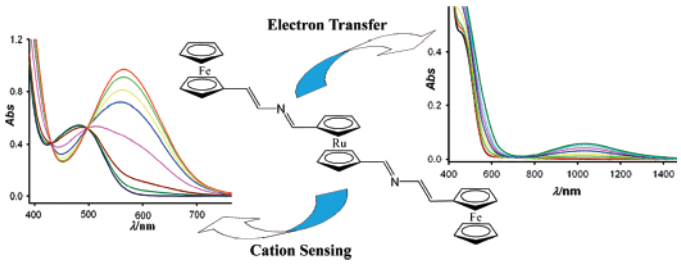

The synthesis, electrochemical, and optical properties of homo- (**5**, **8**, **9**, and **12**) and heterometallic (**6**, **7**, **10**, and **11**) ferrocene-ruthenocene triads, are presented. Triferrocenyl derivatives **5** and **9** form the mixed-valence species $\mathbf{5}^{\bullet+}$ and $\mathbf{9}^{2+}$ by partial oxidation, which show intramolecular electro-transfer phenomena. Interestingly, spectroelectrochemical studies of compound **11**, bearing two peripheral ferrocene units and one central ruthenocene moiety, revealed the presence of low-energy bands in the near-infrared (NIR) region, which indicate a rather unusual intramolecular charge-transfer between the ferrocene and ruthenocene units. The value of the electronic coupling parameter $V_{ab} = 150$ cm^{-1} calculated by deconvolution of the observed Fe(II)−Fe(III) IVCT transition in the mixed-valence compound $\mathbf{11}^{\bullet+}$, ($d_{Fe(II)-Fe(III)} = 18.617$ Å), indicates the ability of the ruthenocene system to promote a long distance intervalence electron-transfer. Moreover, the reported triads show selective cation sensing properties. Triads **5**, **9**, and **11** behave as dual redox and optical chemosensors for Zn^{2+}, Hg^{2+}, and Pb^{2+}. Their oxidation redox peaks are anodically shifted (up to 130 mV), and their low-energy (LE) bands of the absorption spectra are red-shifted (up to 115 nm) upon complexation with these metal cations. These changes in the absorption spectra are accompanied by dramatic color changes which allow the potential for "naked eye" detection.

Introduction

Oligomeric metallocene-based species assembled on π-conjugated frameworks displaying multielectron redox chemistry have attracted much attention with respect to their electrochemical, electronic, and magnetic properties.[1] Although there are many studies on bridged bi(ferrocenyl) systems, in which the well-defined redox chemistry of ferrocene serves as a powerful electrochemical probe to investigate ground-state electronic coupling through space or through bonds,[2] bi(ruthenocenyl) compounds have been much less studied, presumably partly due to the irreversible redox chemistry of ruthenocene itself.[3] Biheterometallocene complexes containing two different types of metal are generally less straightforward to prepare than symmetrical species. This appears to be the reason why they have been studied only in a few cases,[4] and even fewer studies of systems incorporating a conjugated ferrocene-ruthenocene

† Dedicated to Prof. Miguel Yus (Univ. Alicante) on the occasion of his 60th birthday.

(1) (a) Astruc, D. *Acc. Chem. Rev.* **1997**, *30*, 383. (b) Joachim, C.; Gimzewski, J. K.; Aviram, A. *Nature*, **2000**, *408*, 541. (c) Segal, D.; Nitzan, A.; Davis, W. B.; Wasielewski, M. R.; Ratner, M. A. *J. Phys. Chem. B.* **2000**, *104*, 3817. (d) Paddow-Row, M. N. In *Electron Transfer in Chemistry*; Balzani, V., Ed.; Wiley-VCH: Weinheim, 2001; Vol 2, p 179. (e) De Cola, L.; Belser, P. In *Electron Transfer in Chemistry*; Balzani, V., Ed.; Wiley-VCH: Weinheim, 2001; Vol 5, p 97. (f) Kilsa, K.; Kajanus, J.; Macpherson, A. N.; Martensson, J.; Albinsson, B. *J. Am. Chem. Soc.* **2001**, *123*, 3069. (g) Launay, J.-P. *Chem. Soc. Rev.* **2001**, *30*, 386. (h) Newton, M. D. *Chem. Rev.* **1991**, *91*, 767. (i) Nelsen, S. F.; Ismagilov, R. F.; Powell, D. F. *J. Am. Chem. Soc.* **1998**, *120*, 1924. (j) Davis, D. F.; Svec, W. A.; Ratner, M. A.; Wasielewski, M. R. *Nature* **1998**, *396*, 60.

(2) Barlow, S.; O'Hare, D. *Chem. Rev.* **1997**, *97*, 637.

10.1021/jo071066g CCC: $37.00
Published on Web 08/04/2007

framework have been described.[5] Experimental and theoretical studies on higher nuclearity polymetallocene assemblies are relatively scarce, despite the potential of these studies to provide one of the most powerful and sensitive probes to elucidate aspects of intercomponent intramolecular electron-transfer. Only very few electrochemical studies have been published on linear bridged ferrocene triads,[6] whereas the chemistry of trimetallocene triads bearing at least a ruthenocene moiety remains unexplored. The elucidation of multisite effects on electron-transfer phenomena in trimetallocene complexes provides the link between the understanding of such processes in bimetallocene species and in extended arrays and metallosupramolecular systems.

In this context, we have designed triads containing both ferrocene and ruthenocene units as redox centers, linked through aza-conjugated bridges which additionally comprise putative cation-binding sites. These molecular systems would exhibit richer electronic interactions and multiple redox properties because electronic communication would occur between iron and ruthenium redox centers respectively. Furthermore, the electronic effect mediated by the asymmetric bridging ligand is likely tunable not only by altering the relative position of the metallocenes in the bridge, but also by the nature of the central and peripheral metallocene units. In these systems, additionally, the central metallocene could operate as an electron relay providing a much more efficient electron transfer between the two peripheral metallocenes. Eventually, the nitrogen atoms present in the azabridges of this kind of molecules add another interesting and useful function such as its ability to act as metal-ion ligand.[7] Consequently, the preparation of ferrocene, ruthenocene or *mixed* ferrocene-ruthenocene triads, with aza-unsaturated bridges, could be of interest for the construction of homo- or heterotrimetallic systems which can behave not only as suitable models to study the intramolecular charge-transfer across aza-conjugated linkers but also as redox-switching receptors, with the capability of selectively sensing metal-ion guests.

SCHEME 1. Synthesis of Compounds 5, 6, 7, and 8[a]

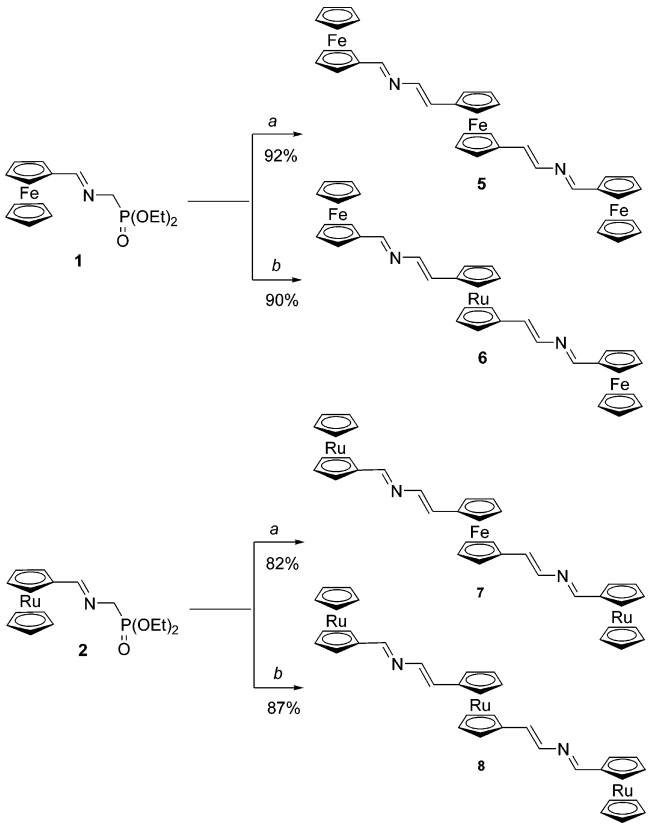

[a] Reagents. (*a*) (i) *n*-BuLi/-78 °C (ii) 1,1′-diformylferrocene; (*b*) (i) *n*-BuLi/-78 °C (ii) 1,1′-diformylruthenocene.

Results and Discussion

Synthesis. The preparation of both homo- (**5**, **8**, **9**, **12**) and heterotrimetallic (**6**, **7**, **10**, **11**) derivatives is outlined in Schemes 1 and 2. Specifically, isomers bearing the central metallocene unit linked to the 4 position of the azadiene bridge (**5**, **6**, **7**, **8**) were prepared starting from the appropriate *N*-substituted diethyl aminomethylphosphonate **1**[8] or **2**.[9] Generation of their corresponding metalloylides, by reaction with *n*-BuLi at −78 °C, and subsequent reaction with the appropriate 1,1′-diformylmetallocene[10] provided the 1,1′-bis(2-aza-1-metallocenyl-1,3-butadien-4-yl)metallocene triads **5**−**8** in excellent yields (82−92%)

(3) (a) Sato, V.; Kudo, A.; Kawata, Y.; Saitoh, H. *Chem. Commun*. **1996**, 25. (b) Sato, M.; Kawata, Y.; Kudo, A.; Iwai, A.; Daitoh, H.; Ochiai, S. *J. Chem. Soc., Dalton Trans*. **1998**, 2215. (c) Watanabe, M.; Sato, M.; Takayama, T. *Organometallics* **1999**, *18*, 5201. (d) Sato, M.; Maruyama, G.; Tanemura, A. *J. Organomet. Chem.* **2002**, *655*, *23*. (e) Sato, M.; Watanabe, M. *Chem. Commun*. **2002**, 1574. (f) Sato, M.; Suzuki, M.; Okoshi, M.; Kurasina, M.; Watanabe, M. *J. Organomet. Chem*. **2002**, *648*, 72. (g) Sato, M.; Nagata, T.; Tanemura, A.; Fujihara, T.; Kamakura, S.; Unoura, K. *Chem.−Eur. J*. **2004**, *10*, 2166. (h) Sato, M.; Kubota, Y.; Kawata, Y.; Fujihara, T.; Unoura, Kei.; Oyama, A. *Chem.−Eur. J*. **2006**, *12*, 2282. (i) Sato, M.; Kubota, Y.; Tanemura, A.; Maruyama, G.; Fujihara, T.; Nakayama, J.; Takayanagi, T.; Takahashi, K.; Unoura, K. *Eur. J. Inorg. Chem.* **2006**, 4577.

(4) (a) Watanabe, M.; Motoyama, I.; Takayama, T. *J. Organomet. Chem.* **1996**, *524*, 9. (b) Neuse, E. W.; Loonat, M. S. *Transition Met. Chem. (Dordrecht, Neth.)* **1981**, *260*, 6. (c) Watanabe, M.; Sano, H. *Chem. Lett.* **1989**, 1345. (d) Watanabe, M.; Sano, H. *Bull. Chem. Soc. Jpn.* **1990**, *63*, 777. (e) Watanabe, M.; Masuda, Y.; Motoyama, I.; Sano, H. *Bull. Chem. Soc. Jpn.* **1988**, *61*, 827. (f) Watanabe, M.; Motoyama, I.; Takayama, T. *Bull. Soc. Chim. Jpn.* **1996**, *69*, 2877.

(5) (a) Obendorf, D.; Schottenberger, H.; Wurst, K.; Schuler, N.; Laus, G. *J. Organomet. Chem*. **2005**, *690*, 811. (b) Caballero, A.; Garcia, R.; Espinosa, A.; Tárraga, A.; Molina, P. *J. Org Chem*. **2007**, *72*, 1161.

(6) (a) Pannell, K. H.; Dementiev, V. V.; Li, H.; Cervantes-Lee, F.; Nguyen, M. T.; Diaz, A. F. *Organometallics* **1994**, *13*, 3644. (b) Barlow, S.; Murphy, V. J.; Evans, J. S. O.; O'Hare, D. *Organometallics* **1995**, *14*, 3461. (c) Rulkens, R.; Lough, A. J.; Manners, I.; Lovelace, S. R.; Grant, C.; Geiger, W. E. *J. Am. Chem. Soc*. **1996**, *118*, 12683. (d) Hirao, T.; Kurashima, M.; Aramaki, K.; Nishihara, H. *J. Chem. Soc., Dalton Trans* **1996**, 2929. (e) Dong, T-Y.; Lee, W-Y.; Su, P-T.; Chang, L-S.; Lin, K-J. *Organometallics* **1998**, *17*, 3323. (f) Tárraga, A.; Molina, P.; Curiel, D.; Velasco, M. D. *Organometallics* **2001**, *20*, 2145. (g) Preliminary communication: Caballero, A.; Tárraga, A.; Velasco, M. D.; Espinosa, A.; Molina, P. *Org. Lett*. **2005**, *7*, 3171. (h) Dong, T-Y.; Chang, S-W.; Lin, S-F.; Lin, M-C.; Wen, Y-S.; Lee, L. *Organometallics* **2006**, *25*, 2018. (i) Wagner, M. *Angew. Chem., Int. Ed.* **2006**, *45*, 5916. (j) Lim, Y-K.; Wallace, S.; Bollinger, J. C.; Chen, X.; Lee, D. *Inorg. Chem.* **2007**, *46*, 1694.

(7) (a) Caballero, A.; Tormos, R.; Espinosa, A.; Velasco, M. D.; Tárraga, A.; Miranda, M. A.; Molina, P. *Org. Lett.* **2004**, *6*, 4599. (b) Caballero, A.; Lloveras, V.; Tárraga, A.; Espinosa, A.; Velasco, M. D.; Vidal-Gancedo, J.; Rovira, C.; Wurst, K.; Molina, P.; Veciana, J. *Angew. Chem., Int. Ed*. **2005**, *44*, 1977. (c) Caballero, A.; Tárraga, A.; Velasco, M. D.; Molina, P. *Dalton Trans.* **2006**, 1390. (d) Martinez, R.; Zapata, F.; Caballero, A.; Espinosa, A.; Tárraga, A.; Molina, P. *Org. Lett*. **2006**, *8*, 3235.

(8) Lloveras, V.; Caballero, A.; Tárraga, A.; Velasco, M. D.; Espinosa, A.; Wurst, K.; Evans, D. J.; Vidal-Gancedo, J.; Rovira, C.; Molina, P.; Veciana, J. *Eur. J. Inorg. Chem.* **2005**, 2436.

(9) Caballero, A.; García, R.; Espinosa, A.; Tárraga, A.; Molina, P. *J. Org. Chem.* **2007**, *72*, 1161.

(10) 1-Formylruthenocene and 1,1′-diformylruthenocene were prepared by mono- and dilithiation of ruthenocene and subsequent reaction with DMF, following a modification of the previously described procedure: Sanders, R.; Mueller-Westerhoff, U. T. *J. Organomet. Chem.* **1996**, *512*, 21.

SCHEME 2. Synthesis of Compounds 9, 10, 11, and 12[a]

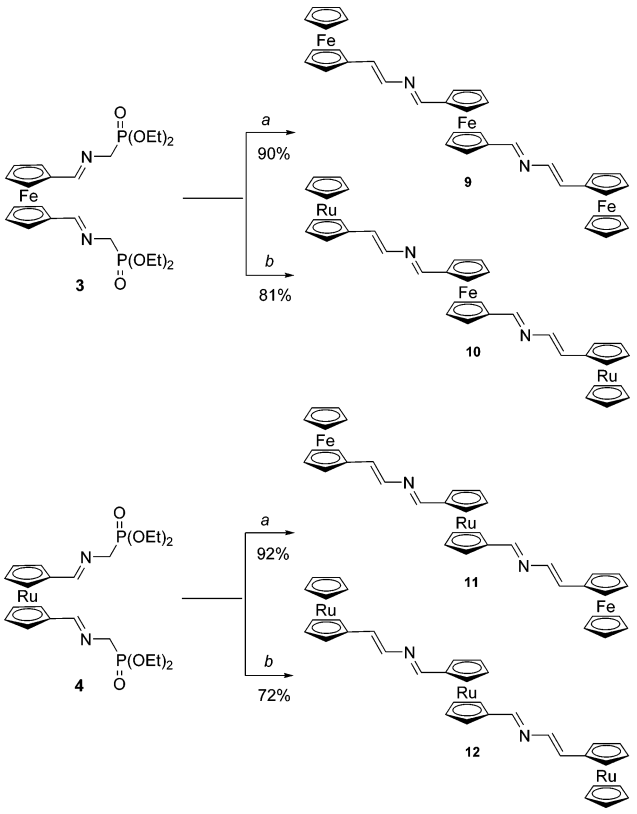

[a] Reagents. (*a*) (i) *n*-BuLi/-78 °C (ii) formylferrocene; (*b*) (i) *n*-BuLi/-78 °C (ii) formylruthenocene.

(Scheme 1). Following the same methodology but only by changing the reaction sequence, the isomeric triads **9**−**12** were prepared. Thus, starting from appropriate 1,1′-metallocenediyl-bis(methylidenaminomethylphosphonate) **3**[7b] or **4**[9] and 1-formylferrocene or 1-formylruthenocene as carbonyl components, the trimetallic derivatives **9**−**12**, with the common structural feature of having the central metallocene subunit linked to the 1 position of the azadiene bridge, were obtained in good yields (72−92%) (Scheme 2).

All these new structural motifs were fully characterized using ^{1}H and ^{13}C NMR and EI or FAB mass spectrometry. In general, the ^{1}H NMR spectra showed the appearance of four pseudotriplets, integrating four protons each, assigned to the 16 protons within the four monosubstituted cyclopentadienenyl (Cp) rings, and the signals corresponding to those ruthenocene protons are deshielded with respect to those located within the ferrocene moiety. The protons present in the 2-aza-1,3-butadiene bridges appeared as one singlet (−C*H*═N−) and two doublets (−C*H*═C*H*−).

Assignment of the configuration of the double bonds present in the 2-aza-1,3-butadiene bridges was achieved by inspection of the corresponding ^{1}H NMR spectroscopic data.[8] The *E*-configuration of the carbon−carbon double bond, as is expected in a Horner-Wadsworth-Emmons olefination process, was confirmed by the value of the vicinal coupling constants. In addition, NOE and two-dimensional NOESY experiments carried out on $CDCl_3$ solutions confirmed the (*E*,*E*)-configuration of the double bonds present in the bridge.

Electrochemical Properties. The redox chemistry of compounds **5**−**12** was investigated by cyclic (CV) and differential pulse (DPV) techniques, carried out in a CH_3CN/CH_2Cl_2 (3/2, v/v) solution and using [*n*-Bu_4N]PF_6 (0.15 M) as the supporting electrolyte. The electrochemical data, which are summarized in Table 1, revealed characteristic general features. All the triads described show electroactivity due both to the presence of the three metallocenyl units and to the oxidation of the 2-aza-1,3-butadiene bridge. Thus, in the range 0−0.9 V, they show two oxidation waves corresponding to the oxidation of the metallocene subunits. Upon scanning to higher potential (1.5 V), a clearly irreversible wave appeared in the range 0.95−1.4 V vs decamethylferrocene (DMFc), which was attributed to the aza-bridges oxidation. As regards as the redox behavior of the ferrocene moieties is concerned, the oxidation potentials of the peripheral ferrocenyl units are strongly dependent on the position of the 2-aza-diene bridge to which they are attached, the oxidation being easier than when the ferrocene is linked to the 4 position of the bridge than when it is linked to the 1 position, e.g., for compound **9** (4-ferrocenyl substituted) $E_p = 0.51$ V vs DMFc and for compound **5** (1-ferrocenyl substituted) $E_p = 0.69$ V vs DMFc. The influence of the central metallocene unit on the oxidation potentials of the peripheral ferrocene moieties also depends on the position at which the organometallic fragments are linked to the unsymmetrical azabridge: for 1-ferrocenyl substituted triads **5** and **6**, the central ferrocene unit in **5** makes the oxidation of the peripheral ferrocene ($E_p = 0.69$ V vs DMFc) easier than the ruthenocene makes it in compound **6** ($E_p = 0.78$ V vs DMFc), whereas for 4-ferrocenyl substituted triads **9** and **11**, both central metallocenes have the same effect (Table 1). By comparison of the oxidation potentials of the peripheral ferrocenyl units in the homotrimetalic triads **5** and **9** with those found for the ferrocenyl units in the same position of the bridge in the 1,4-bis(ferrocenyl)-2-aza-1,3-butadiene[8] ($\Delta E_{1/2} = 0.56$ and 0.77 V vs DMFc), it is easy to conclude that the presence of a central ferrocene moiety in **5** and **9** results in a decrease of the oxidation potential both of the 1-ferrocenyl units in **5** (0.69 vs 0.77 V) and 4-ferrocenyl units in **9** (0.51 vs 0.56 V).

TABLE 1. Electrochemical Data of Triads 5−12

comp.	^1E_p[a]	^2E_p[b]	ΔE_p[c]	^3E_p[d]	K_c
5	0.69[e]	0.47[e]	0.22	1.12	5.20×10^3
6	0.78[f]	0.56[f]	0.22	1.18	
7	0.79[f]	0.50[f]	0.29	0.90	
8	0.69[f]	0.69[f]	0.000	1.30	
9	0.51[e]	0.84[e]	0.33	1.02	3.79×10^5
10	0.54[f]	0.73[f]	0.19	0.95	
11	0.50[e]	0.92[e]	0.42	1.40	1.26×10^7
12	0.61[f]	0.61[f]	0.000	1.13	

[a] Oxidation potentials corresponding to the terminal metallocene units, in V, vs decamethylferrocene (DMFc). [b] Oxidation potentials corresponding to the central metallocene unit, in V, vs DMFc. [c] $|^1E_p - {}^2E_p|$ in V. [d] Oxidation potential corresponding to the 2-aza-1,3-butadiene bridge, in V, vs DMFc. [e] Reversible oxidation process. [f] Irreversible oxidation process.

Quantum chemical calculations at the DFT level (see the Supporting Information) has allowed satisfactory explanation about the different behavior of the studied systems upon oxidation. The greater ease of oxidation of ferrocene moieties in relation to the ruthenocene analogous, as well as of a metallocene unit at the 4-position in the azadiene bridge in relation to the same type of metallocene linked at the 1-position, has been previously argued elsewere[9] under the theoretical point of view. We have found of high diagnostic interest the study of electric charge variation and Mulliken spin density variation along the oxidative sequence at relevant parts of the molecule (Figure 1). For that purpose, every molecular system in

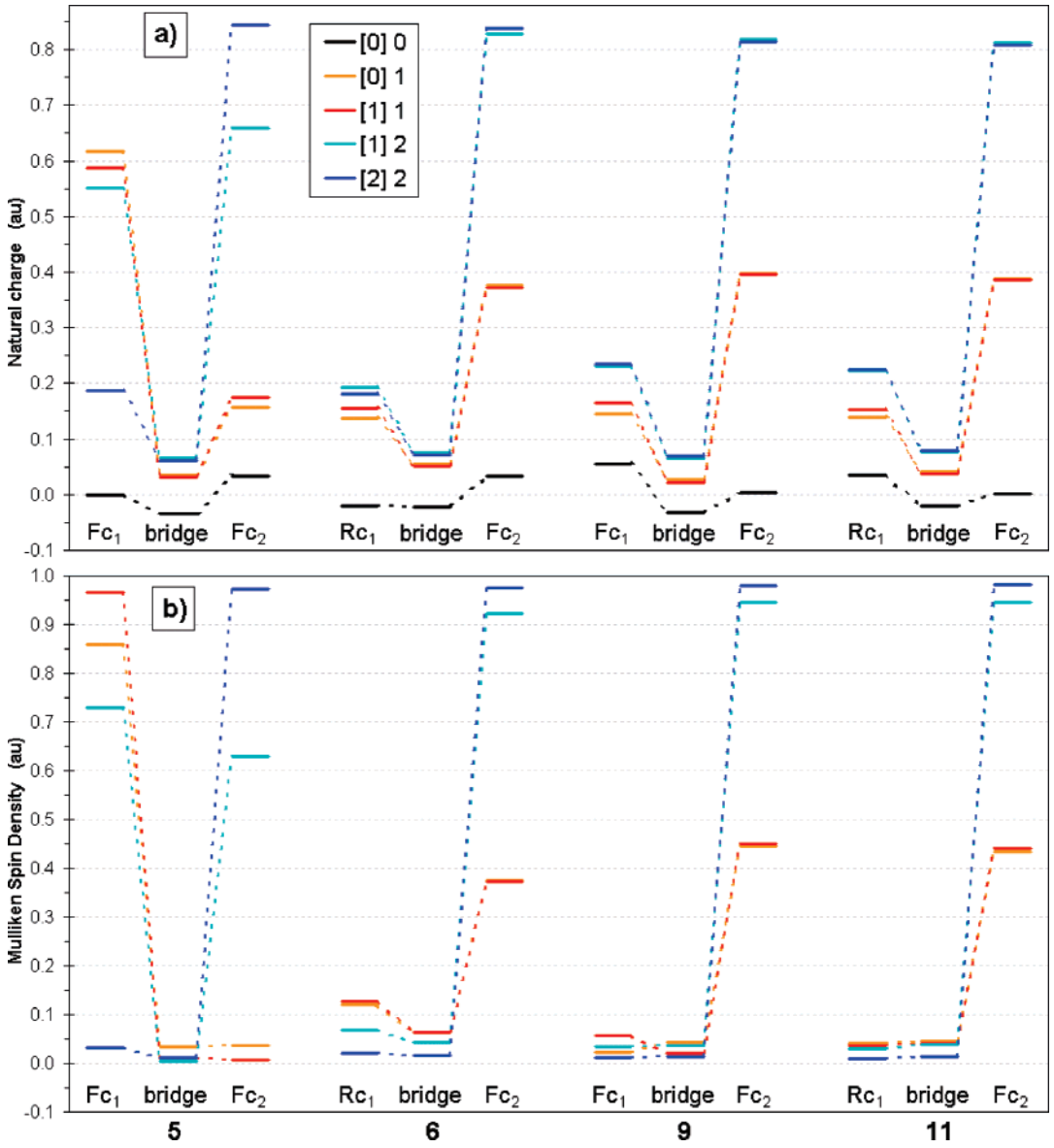

FIGURE 1. Calculated distribution of (a) natural charge and (b) Mulliken spin density in all studied compounds in their neutral form (black), mono-oxidized forms before (orange) and after (red) structural relaxation, and di-oxidized species before (cyan) and after (blue) structural relaxation.

compounds **5**, **6**, **9**, and **11** has been divided in three different subunits: two metallocenyl moieties, the central metallocene Mc_1 and the two peripheral ferrocenes Fc_2, and the two identical bridges connecting them, e.g., sketched as Mc_1(-bridge-Fc_2)$_2$. Electric charges have been obtained from the NBO (Natural Bond Order) analysis and computed for every single metallocene or bridge subunit. We have made the assumption that the two first one-electron oxidative processes can be divided into five steps which can be taken as happening successively. They have been named as *[n]m* where the first index between brackets denotes the employed geometry optimized for the system having a net charge "*n*", and the second one refers to the actual charge "*m*" of the system under consideration. Thus, starting from the neutral optimized structures ([0]0), removal of one electron from the HOMO leads to an unstable radical-cation state ([0]1) with instantaneously redistributed electron density and which thereafter reorganizes its geometry ([1]1) to better accommodate the generated electronic deficiency. Analogously, subsequent removal of a second electron would lead consecutively to dications [1]2 and [2]2.

Several conclusions can be extracted from the inspection of Figure 1. In the neutral form all azadiene bridges display an small charge (range −0.033 to −0.021), with the metallocene at the 1-position of the bridge having more positive charge (range 0.033 to 0.056 au) than the other at the 4-position (range −0.020 to 0.004 au), thus indicating the tendency of the azadiene bridge to push electron density in the C(1) → C(4) sense (Figure 1a). As outlined before, compounds **9** and **11**, having the central metallocene unit Mc_1 linked to the 1-position of the azadiene bridges, are expected to display roughly the same oxidative behavior, taking place both one and two-electrons removal from the peripheral Fc_2 units in the same extent with minimal structural reorganization ([0]1 → [1]1 and [1]2 → [2]2) and maintaining the rest of the molecule virtually unoxidized (only residual spin density over Mc_1 and the bridges, as observed in Figure 1b). On the contrary, important differences can be predicted from theoretical data when the central metallocene Mc_1 is linked to the 4-position of the bridges, as in compounds **5** and **6**. In the triferrocenyl derivative **5**, removal of the first electron should take place from the central more electron rich

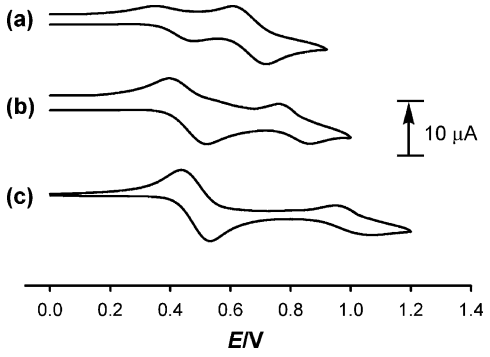

FIGURE 2. CV of compounds (a) **5**, (b) **9**, and (c) **11** (1 mM) in CH_3CN/CH_2Cl_2 (3/2, v/v) using $[(n\text{-}Bu)_4N]PF_6$ (0.1 M) as supporting electrolyte scanned at 100 mV s^{-1}.

(less positively charged) Fc_1 unit, which becomes fully oxidized upon reorganization with only residual oxidation on the bridges and periheral Fc_2 units. The next one-electron oxidation (and the next oxidative step, not shown) takes place on the external Fc_2 moieties. Nevertheless, compound **6** behaves differently, showing an oxidative behavior very much resembling that of the regioisomer **11**: the first two electrons are removed mainly from the Fc_2-centered HOMOs but with additional small but significative oxidation of both the central Rc_1 unit and the azadiene bridges (Figure 1). The above electronic changes upon oxidation can also be characterized by the variation of proper geometrical distortion parameters at the metallocene units mainly the M···Cp distances (see the Supporting Information) and the degree of bond-length alternation within Cp units.

Additionally, this structural feature concerning the position of the 2-aza-diene bridge to which the external ferrocene units are attached seems to also have influence in the reversibility of the oxidation processes involved. The ruthenocene oxidation significantly reduced the reversibility of the Fe(II)/Fe(III) redox couple. Thus, in compound **6**, the partial oxidation of both the central ruthenocene unit and the azadiene bridges ($E_p = 0.56$ V), as shown before, seems to make the oxidation process of the peripheral ferrocene units ($E_p = 0.78$ V) irreversible. However, in compound **11**, the wave associated to the oxidation of the peripheral ferrocene moieties ($E_p = 0.50$ V) is completely reversible ($\Delta E_p = 0.60$ V)[11] because it takes place before the central ruthenocene center is oxidized ($E_p = 0.92$ V) in a rather unusual quasi-reversible way ($\Delta E_p = 0.11$ V) (Figure 2). This electrochemical behavior of the ruthenocene unit in compound **11** is unexpected, because it is well-known that ruthenocene and its derivatives usually undergo an irreversible one-step two-electron oxidation process,[12] and only a few examples of a quasi-reversible one-electron oxidation of ruthenocene derivatives have been reported.[9,13] On the other hand, it is worth mentioning that while the triferrocene derivatives **5** and **9** show two reversible waves assigned to the oxidation of the two different ferrocene subunits present in their structures, oxidation of the ruthenocene moieties in the case of the triruthenocene derivatives **8** and **12** give only rise to one irreversible wave at $E_p = 0.69$ V and $E_p = 0.61$ V vs DMFc, respectively, which is in agreement with the results previously reported for related ruthenocene dyads linked by a single 2-aza-diene bridge.[9]

Moreover, it is important to underline the large potential shift ($\Delta E_p = 0.42$ V) observed between the two oxidation processes involved in the heterotrimetallic derivative **11**, which reflects, in principle, some sort of electronic delocalization along this system. The stability of the mixed-valence species $\mathbf{11}^{2+}$ can be initially estimated from the equilibrium constant $K_c = \exp[\Delta E_{1/2}F/RT]$ which is evaluated from this electrochemical data as $K_c = 1.26 \times 10^7$ (Table 1). Nevertheless, it is very well-established that the $\Delta E_{1/2}$ values alone represents only a poor quantitative parameter for the assessment of the extent of the metal−metal interaction, because this magnitude has been shown to be extremely medium-dependent[14] and, as a consequence investigations in the near-IR region at which mixed-valence species typically absorb, have also been carried out.

Optical and Spectroelectrochemical Properties. The UV−vis data of triads **5**−**12** were recorded as 10^{-3} M solutions in CH_2Cl_2. In general, the electronic absorption spectra of these compounds are characterized by the presence of two prominent high energy (HE) absorption bands with a maximum between 256 and 288 nm and between 293 and 337 nm, respectively, which are assigned to a localized $\pi-\pi^*$ excitation mainly within the 2-aza-1,3-butadiene bridge. In addition to this band, another weaker absorption bands are visible, which can be explained on the basis of the individual ferrocene and ruthenocene components that are present in each trimetallocene. Thus, the presence of a low-energy (LE) band between 363 and 367 nm, observed in the ruthenocene triads **8** and **12** and in the heterotrimetallic derivative **10**, could be ascribed to a Ru^{II}-to-ligand (MLCT) transition.[15] On the other hand, the other trimetallic derivatives bearing ferrocene moieties (**5**−**7** and **9**−**11**) also showed another weaker low-energy absorption between 456 and 485 nm that is assigned to another localized excitation, with a lower energy, produced either by two nearly degenerate transitions, an Fe^{II} d−d transition,[11] or a Fe^{II}-to-ligand (MLCT) process ($d_\pi-\pi^*$) (LE band). This assignment is in accordance with the latest theoretical treatment (model III) reported by Barlow et al.[16] (Table 2).

The generation of the oxidized species derived from the triads **5**−**12** was performed either chemically or elctrochemically and monitored by absorption spectroscopy. Stepwise coulometric titrations were performed on *ca*. 10^{-3} M solutions of the ligands studied in CH_2Cl_2, with $[(n\text{Bu})_4N]PF_6$ (0.15 M) as supporting

(11) The criteria applied for reversibility was (i) separation of 60 mV between cathodic and anodic peaks, (ii) close-to-unity ratio of the intensities of the cathodic and anodic currents I_c/I_a, and (iii) constancy of the half-wave potential on changing sweep rate in CVs. The same half-wave potential values have been obtained from the DPV peaks and from an average of the cathodic and anodic cyclic voltammetry peak.

(12) (a) Kuwana, T.; Bublitz, D. E.; Hoh, G. *J. Am. Chem. Soc*. **1960**, *82*, 5811. (b) Gubin, S. P.; Smirnova, L. I.; Denisovich, L. I.; Lubovich, A. A. *J. Organomet. Chem.* **1971**, *30*, 243. (c) Denisovich, L. I.; Zakurin, N. V.; Bazrukova, A. A.; Gubin, S. P. *J. Organomet. Chem*. **1974**, *81*, 207.

(13) (a) Gale, R. J.; Job, R. *Inorg. Chem. 1981*, *20*, *42*. (b) Hill, M. G.; Lamanna, W. M.; Mann, K. R. *Inorg. Chem*. **1991**, *30*, 4687. (c) Koelle, U.; Salzer, A. *J. Organomet. Chem.* **1983**, *243*, C27. (c) Koelle, U.; Grub, J. *J. Organomet. Chem.* **1985**, *289*, 133.

(14) (a) Barriere, F.; Camire, N.; Geiger, W. E.; Mueller-Westerhoff, U. T.; Sanders, R. *J. Am. Chem. Soc*. **2002**, *124*, 7262. (b) Jones, S. C.; Hascall, T.; Barlow, S.; O'Hare, D. *J. Am. Chem. Soc.* **2002**, *124*, 11610. (c) Yeung, L. K.; Kim, J. E.; Chung, Y. K.; Rieger, P. H.; Sweigart, D. A. *Organometallics* **1996**, *15*, 3891.

(15) (a) Sohn, Y. S.; Hendrickson, D. N.; Gray, M. B. *J. Am. Chem. Soc*. **1971**, *93*, 3603. (b) Sanderson, C. T.; Quinian, J. A.; Conover, R. C.; Johnson, M. K.; Murphy, M.; Dluhy, R. A.; Kuntal, C. *Inorg. Chem*. **2005**, *44*, 3283. (c) Gao, L.-B.; Zhang, L.-Y.; Shi, L.-X.; Cheng, Z.-N. *Organometallics*, **2005**, *24*, 1678.

(16) (a) Barlow, S.; Bunting, H. E.; Ringham, C.; Green, J. C.; Bublitz, G. U.; Boxer, S. G.; Perry, J. W.; Marder, S. R. *J. Am. Chem. Soc*. **1999**, *121*, 3715. (b) Yamaguchi, Y.; Ding, W.; Sanderson, C. T.; Borden, M. L.; Morgan, M. J.; Kutal, C. *Coord. Chem. Rev.* **2007**, *251*, 515.

TABLE 2. UV−Visible−Near-IR Data in CH_2Cl_2

comp.	λ_{max} [nm] (10^{-3} ϵ [$M^{-1}cm^{-1}$])
5	256 (20.80), 333 (15.10), 483 (5.30)
$\mathbf{5}^{+a}$	358 (16.32), 558 (5.70), 1296[b] (0.14)
$\mathbf{5}^{3+a}$	364 (14.02), 565 (5.40), 750[b] (4.40), 1059[b] (4.60)
6	256 (24.04), 337 (31.50), 456 (4.35)
$\mathbf{6}^{3+a}$	352 (11.65), 532 (4.50)
7	278 (sh), 316 (23.0), 466 (2,90)
$\mathbf{7}^{3+a}$	349 (12.1), 414 (sh), 927(0.28)
8	306 (24.82), 364 (sh)
$\mathbf{8}^{3+a}$	286 (13.00), 329 (13.40), 432 (11.50)
9	258 (23.45), 336 (31.20), 485 (6.08)
$\mathbf{9}^{2+a}$	374 (19.10), 577 (6.60), 750[b] (0.50), 950[b] (0.12), 1228[b] (0.30)
$\mathbf{9}^{3+a}$	259 (13.77), 287 (sh), 546 (4.40), 750[b] (0.60), 950[b] (0.40)
10	288 (14.15), 328 (15.25), 363 (sh), 477 (1.70)
$\mathbf{10}^{3+a}$	341 (5.04), 367 (sh), 469 (sh), 527 (sh)
11	268 (20.55), 325 (31.90), 455 (4.20)
$\mathbf{11}^{+a}$	252 (20.50), 324 (26.85), 438 (sh), 1026[b] (0.60)
$\mathbf{11}^{2+a}$	348 (15.98), 422 (sh), 541 (4.70), 1242[b] (0.45)
$\mathbf{11}^{3+a}$	352 (9.35), 427 (sh), 870 (0.63)
12	293 (7.90), 367 (sh)
$\mathbf{12}^{3+a}$	363 (4.95), 455 (3.40)

[a] Oxidized species obtained electrochemically in CH_2Cl_2 (10^{-3} M) using [*n*-Bu_4N]PF_6 (0.15 M) as the supporting electrolyte. [b] Values obtained by deconvolution of the experimental spectra.

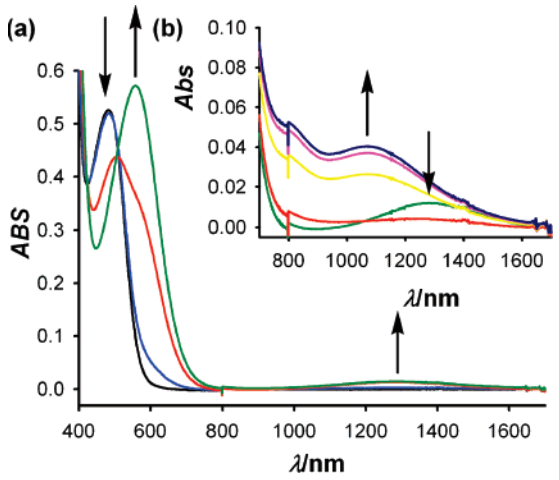

FIGURE 3. Evolution of UV−vis−NIR spectra during the course of the oxidation of compound **5** (1 mM) in CH_2Cl_2 with [(*n*-Bu) $_4$N]PF_6 (0.15 M) as supporting electrolyte when: (a) $0 \le n \le 1$; (b) $1 \le n \le 3$ electrons are removed. Arrows indicate absorptions that increase or decrease during the experiment.

electrolyte, and the absorption spectra were regularly recorded for different average numbers of removed electrons.

Thus, the formation of the oxidized species derived from **5** and **9** was performed either by chemical oxidation with the appropriate amount of silver trifluoromethanesulfonate or by constant potential electrolysis, 0.12 V above $E_{1/2}$ of the first ferrocenyl redox couple (0.59 V for **5** and 0.63 V for **9**), and monitored by absorption spectroscopy (see the Supporting Information). During the oxidation of the central ferrocenyl subunit in **5** (0−1 range of removed electrons) a new LMCT (Cp−Fe(III)) band at $\lambda = 558$ nm ($\epsilon = 5700$ M^{-1} cm^{-1}) appears with concomitant decreasing of the band at $\lambda = 483$ nm ($\epsilon = 5300$ M^{-1} cm^{-1}) (Figure 3). Moreover, in the NIR region, a new and weak band at $\lambda = 1296$ nm ($\epsilon = 140$ M^{-1} cm^{-1}) appears, increasing continuously its intensity until one electron is removed, and which is assigned to a bridge-mediated superexchange process between the two different coupled iron sites Fe(III) and Fe(II) (intervalence charge-transfer band, IVCT). Along with these changes, well-defined isosbestic points at $\lambda = 424$ nm and $\lambda = 509$ nm are maintained during the course of the oxidation process. Interestingly, on removing more electrons (from 1 to 3 at a constant potential of 0.81 V), the intensity of the IVCT band at $\lambda = 1296$ nm decreases until it disappears when the compound is fully oxidized but, at the same time, two new bands appear at $\lambda = 750$ nm ($\epsilon = 440$ M^{-1} cm^{-1}) and $\lambda = 1059$ nm ($\epsilon = 460$ M^{-1} cm^{-1}), which could be attributed to LMCT transitions from the bridge to Fe(III) (Figure 3b). Similar low-energy transitions have also been observed in other aza-substituted ferrocenes which after electrochemical oxidation of the Fe(II) show intramolecular electron-transfer transitions between the nitrogen atom of the aza-substituent and the Fe(III) centers.[17]

During the oxidation of **9** at a constant potential of 0.63 V ($0 \le n \le 2$), the band located at $\lambda = 485$ nm progressively dissapears and, at the same time, a new band at $\lambda = 577$ nm ($\epsilon = 6600$ M^{-1} cm^{-1}), assigned to LMCT transitions, continuously increases in intensity reaching a maximum when two electrons have been removed. Along with the changes of these bands, two well-defined isosbestic points at $\lambda = 450$ and 511 nm are maintained during the course of the oxidation process (see the Supporting Information). Nevertheless, the most interesting feature detected is that during the formation of the dication $\mathbf{9}^{2+}$, three new bands appear at the near-IR, at $\lambda = 750$ nm ($\epsilon = 500$ M^{-1} cm^{-1}), $\lambda = 950$ nm ($\epsilon = 120$ M^{-1} cm^{-1}), and $\lambda = 1228$ nm ($\epsilon = 300$ M^{-1} cm^{-1}). On removing more electrons ($2 \le n \le 3$) at a constant potential of 0.96 V, the intensity of the first two bands continues increasing whereas the band at 1228 nm decreases until it disappears when the fully oxidized system is completely formed (see the Supporting Information). These experimental facts suggest that the absorption bands at $\lambda = 750$ and 950 nm could be due to LMCT transitions from the bridge to Fe(III), whereas the band at $\lambda = 1228$ nm could be attributed to a bridge-mediated superexchange process between the two peripheral Fe(III) and the central Fe(II) (IVCT band). Table 2 collects all the spectra data for oxidized complexes $\mathbf{9}^{2+}$ and $\mathbf{9}^{3+}$.

By contrast to the above-described behavior shown by the triferrocenes **5** and **9**, the structurally related linear triruthenocene derivatives **8** and **12**, which only display one irreversible oxidation wave in their CVs, do not display any band in the near-IR (NIR) region, when they were oxidized at a constant potential of 0.81 and 0.74 V, respectively. These results indicate, as it was expected, that the three ruthenium centers were oxidized at the same potential and, therefore, a mixed-valence complex is not formed.

Because of the nonreversible features of the CVs of ferrocene-rutenocene triads **6**, **7**, and **10**, all attempts to promote a controlled oxidation process failed. Then, the full oxidized compounds were only obtained in these cases which, in turn, did not display any NIR absorption band.

Interestingly, the generation of the monooxidized species derived from the heterotrimetallic derivative **11**, bearing two peripheral 4-ferrocenyl units and one central ruthenocene moiety, was performed by constant potential electrolysis at 0.63 V and monitored by absorption spectroscopy. During the oxidation ($0 \le n \le 1$), the band observed in compound **11** at $\lambda = 455$ nm progressively disappears and, at the same time, a new and weak absorption band appears in the NIR region, at $\lambda = 1026$ nm (ϵ

(17) (a) Horie, M.; Suzaki, Y.; Osakada, K. *J. Am. Chem. Soc.* **2004**, *126*, 3684. (b) Horie, M.; Sakano, T.; Osakada, K.; Nakao, H. *Organometallics* **2004**, *23*, 18.

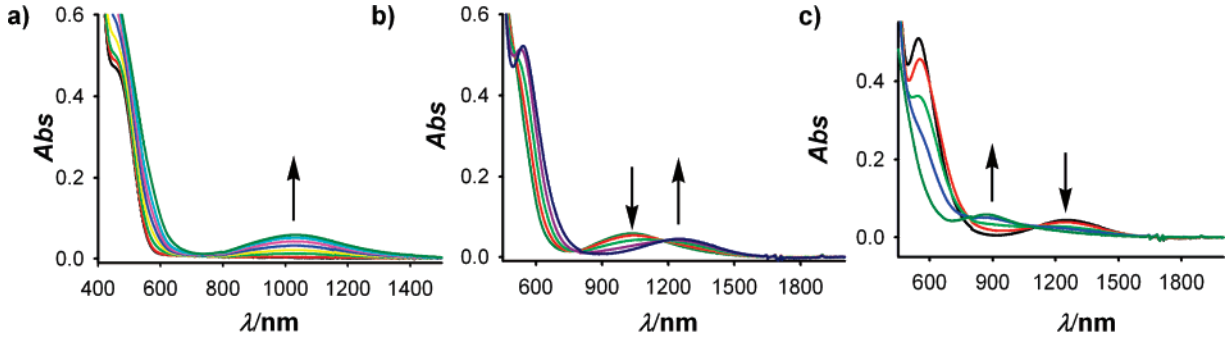

FIGURE 4. Evolution of UV−vis−NIR spectra during the course of the oxidation of compound **11** (1 mM) in CH_2Cl_2 with $[(n\text{-Bu})_4N]PF_6$ (0.15 M) as supporting electrolyte when: (a) $0 \le n \le 1$, (b) $1 \le n \le 2$; (c) $2 \le n \le 3$ electrons are removed. Arrows indicate absorptions that increase or decrease during the experiment.

$= 587\ M^{-1}\ cm^{-1}$), its intensity continuously increasing until one electron is removed and which is assigned principally to IVCT from the Fe(II) to Fe(III) sites although a metal−metal charge transfer (MMCT) from Ru(II) to one peripheral Fe(III) center cannot be discarded. Along with the changes of these bands, a defined isosbestic point at $\lambda = 397$ nm is maintained during the course of the oxidation process. On removing two electrons ($1 \le n \le 2$) at the same constant potential of 0.63 V, the intensity of this band decreases until it disappears when the dioxidized $\mathbf{11}^{2+}$ species is completely formed. Simultaneously, a new band at $\lambda = 1242$ nm ($\epsilon = 450\ M^{-1}\ cm^{-1}$) appears, which is also assigned to a MMCT transition from the Ru(II) to the two peripheral Fe(III) centers. Similar evolution of the vis−NIR spectra has been found during the electrochemical oxidation of the close related 1-ruthenocenyl-4-ferrocenyl-2-aza-1,3-butadiene.[9] Finally, on removing three electrons ($2 \le n \le 3$) by a constant potential electrolysis at 1.05 V, the band at $\lambda = 1242$ nm decreases until complete disappearance when the compound is fully trioxidized $\mathbf{11}^{3+}$ system is formed; at the same time, a new band appears at $\lambda = 870$ nm ($\epsilon = 630\ M^{-1}\ cm^{-1}$), which could be attributed to a ligand−Ru(III) charge transfer (LMCT) transition.[18] Five well-defined isosbestic points at $\lambda = 369$, 450, 504, 794, and 1177 nm are maintained during the course of this oxidation process (Figure 4). The same results were also obtained when the chemical oxidations were carried out by using one, two, or three equivalents of silver trifluoromethanesulfonate as an oxidizing agent, respectively.

The presence of several NIR bands in the spectrum of a mixed-valence complex is not uncommon, and their occurrence is generally explained by means of a strong spin−orbit coupling effect,[19] the presence of a double-exchange mechanism,[20] or the presence of a bridge with accessible electronic state levels or with redox-active bridges.[21]

Although the comproportionation constant K_c and the free energy of comproportionation, $\Delta G_c°$, provide measures for determining the degree of electronic delocalization,[22] previous reports have emphasized that spectral measurements of the IVCT transitions often serve as a more subtle and accurate probe for the degree of electronic coupling.[23] The spectral parameters of the bands present in the NIR, energy (ν_{max}), intensity (ϵ_{max}), and half-bandwidth ($\Delta\nu_{1/2}$), obtained by deconvolution of the experimental spectra performed on spectral intensity times wavenumber vs wavenumber assuming Gaussian shapes, have been used to determine the effective electronic coupling (V_{ab}) and the activation energy of the thermal electron transfer ($\Delta G^{\ddagger}$) through the two-state classical Marcus−Hush theory.[24]

According to Robin and Day classification,[25] mixed-valence compounds are classified in three categories: class I, where the redox centers are completely localized and behave as separate entities; class II, where an intermediate coupling between the mixed-valence centers exists; and class III, where the system is completely delocalized and the redox centers show intermediate valence states. Recently, Meyer[26]defined borderline class II/class III systems, which exhibit both delocalised and localized behavior. Hush theory[27] indicates that, for a class II mixed-valence system with two identical redox centers, the energy of the IVCT transition, ν_{max}, is equal to the sum of the inner and outer-sphere reorganization energies, λ. Where the two redox centers are inequivalent, the relationship is given by $\nu_{max} = \lambda + \Delta G°$, where $\Delta G°$ is the free-energy difference between the initial and the final state after the electron transition, and is usually approximated as the separation ΔE_p of the redox potentials of the processes centered on the isolated units involved in the electron transfer.[28] Thus, the magnitude of the $\Delta G°$ can be obtained by converting the electrochemical value of ΔE_p values into energy units. However, to estimate the most accurately possible $\Delta G°$ values, the appropriate corrections on the values of the redox potentials of the metallocene centers present in these triads have to be made (Table 3). In the case of heterobimetallic complexes, the $\Delta E_{1/2}$, which is indicative

(18) Gao, L-B.; Zhang, L.-Y.; Shi, L.-X.; Chen, Z.-N. *Organometallics* **2005**, *24*, 1678.
(19) (a) Kober, E. M.; Goldsby, K. A.; Narayane, D. N. S.; Meyer, T. J. *J. Am. Chem. Soc.* **1983**, *105*, 4303. (b) Lay, P. A.; Magnuson, R. H.; Taube, H. *Inorg. Chem.* **1988**, *27*, 2364. (c) Laidlaw, W. M.; Denning, R. G. *J. Chem. Soc., Dalton Trans.* **1994**, 1987.
(20) (a) Richardson, D. E.; Taube, H. *J. Am. Chem. Soc.* **1983**, *105*, 40. (b) Halpern, J.; Orgel, L. E. *Discuss. Faraday Soc.* **1960**, *29*, 32.
(21) Nelsen, S. F.; Ismagilov, R. F.; Powell, D. F. *J. Am. Chem. Soc.* **1998**, *120*, 1924.
(22) (a) Creutz, C. *Prog. Inorg. Chem.* **1983**, *30*, 1. (b) Richardson, D. E.; Taube, H. *Coord. Chem. Rev.* **1984**, *60*, 107.
(23) (a) Hush, N. S. *Prog. Inorg. Chem.* **1967**, *8*, 391. (b) Hush, N. S. *Electrochim. Acta* **1968**, *13*, 1005.
(24) Allen, C. C.; Hush, N. S. *Prog. Inorg. Chem.* **1967**, *8*, 357.
(25) Robin, M.; Day, P. *Adv. Inorg. Chem.* **1967**, *10*, 247.
(26) Chen, P.; Meyer, T. J. *Chem. Rev.* **1998**, *98*, 1439.
(27) Hush, N. S. *Coord. Chem. Rev.* **1985**, *64*, 135.
(28) (a) Barlow, S. *Inorg. Chem.* **2001**, *40*, 7047. (b) Albinati, A.; Fabrizi de Biani, F.; Leoni, P.; Marchetti, L.; Pasquali, M.; Rizzato, S.; Zanello, P. *Angew. Chem., Int. Ed.* **2005**, *44*, 5701. (c) Santi, S.; Orian, Durante, L., C.; Bisello, A.; Benetollo, F.; Crociani, L.; Ganis, P.; Ceccon, A. *Chem.−Eur. J.* **2007**, *13*, 1955.

TABLE 3. Parameters Related to the IVCT Bands of Mixed-Valence 5, 9, and 11 Systems

comp.	ν_{max} (cm^{-1})	ϵ_{max} ($M^{-1}cm^{-1}$)	ΔG^{0a} (cm^{-1})	λ (cm^{-1})	$\Delta\nu_{1/2\ exp}$ (cm^{-1})	$\Delta\nu_{1/2\ theo}$ (cm^{-1})	V_{ab} (cm^{-1})	α	$\Delta G^{\ddagger HardReturn}$($cm^{-1}$)	Γ
$\mathbf{5}^{\bullet+}$	7716	140	1669	6046	2785	3737	122	0.016	2346	0.25
$\mathbf{9}^{2+}$	8143	270	1693	6449	3886	3860	201	0.025	2381	0.006
$\mathbf{11}^{\bullet+}$	9746	587	–	9746	3356	4744	152	0.016	–	0.30
$\mathbf{11}^{2+}$	8050	450	2968	5082	2040	3426	182	0.023	–	0.40

[a] $\Delta G°$ in cm^{-1} has been calculated from the values obtained for ΔE_p in volts ($\Delta G° = 8065.54 \times \Delta E_p$), taking into account the E_p values for the reference mononuclear complexes; thus, for $\mathbf{5}^{\bullet+}$: $\Delta E_p = E_p(\mathbf{13}) - E_p(\mathbf{15}) = 0.70 - 0.49 = 0.207$ V; for $\mathbf{9}^{2+}$: $\Delta E_p = E_p(\mathbf{16}) - E_p(\mathbf{14}) = 0.74 - 0.53 = 0.21$ V; for $\mathbf{11}^{2+}$: $\Delta E_p = E_p(\mathbf{17}) - E_p(\mathbf{14}) = 0.90 - 0.53 = 0.37$ V.

of the metal−metal interactions, is no longer the difference between the two subsequent reversible redox waves, but it is the difference between the redox potential of the reversible second wave and the redox potential of the reversible wave of the corresponding monometallic species.[29] In this sense, the oxidation potential of the previously reported[8] mononuclear complexes **13**−**17** have been obtained.

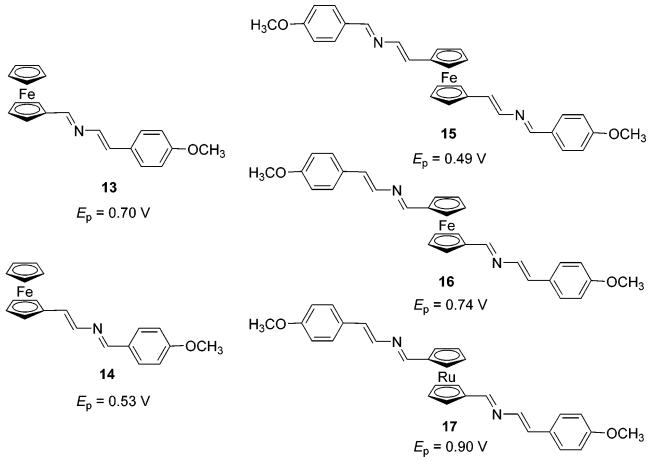

For the class II regime, the $\Delta\nu_{1/2\ theo}$ and the electronic coupling V_{ab} are derived from the Hush equations $\Delta\nu_{1/2\ theo} = (2310\nu_{max})^{1/2}$ and $V_{ab} = (0.0205/d_{ab})(\epsilon_{max}\nu_{max}\Delta\nu_{1/2})^{1/2}$, where d_{ab} is the diabatic metal−metal distance (i.e., the intermetal distance in the hypothetical absence of electronic coupling). Additionally, the delocalisation coefficient α, which is a parameter that quantifies the degree of valence delocalisation in the ground state, (i.e., the fraction of valence electronic charge transferred from the donor to the acceptor metal centers), can be calculated by using the equation $\alpha = V_{ab}/\nu_{max}$.[30] Provided that $V_{ab} < (\lambda + \Delta G°)$ and $|\Delta G°| < \lambda$[31] for an unsymmetrical Class II mixed-valence species, the thermal barrier $\Delta G^{\ddagger}$ is given by eq 1.[30b] Finally, the magnitude of the Γ parameter [$\Gamma = 1 - (\Delta\nu_{1/2\ exp}/\Delta\nu_{1/2\ theo})$] has been used to distinguish the class of mixed-valence system: $0 < \Gamma < 0.1$ indicate the presence of a weakly coupled class II systems; $0.1 < \Gamma < 0.5$ are tipycal for moderately coupled class II systems; $\Gamma = 0.5$ for the systems at the transition between class II and class III; and $\Gamma > 0.5$ for class III mixed-valence systems.[32]

$$\Delta G^{\ddagger} = \frac{\lambda}{4} + \frac{\Delta G_0}{2} + \frac{\Delta G_0^2}{4(\lambda - 2V_{ab})} - V_{ab} + \frac{V_{ab}^2}{(\lambda + \Delta G_0)} \qquad (1)$$

Parameters that have been used to clasify the different mixed-valence species obtained are collected in Table 3. In partially oxidized $\mathbf{5}^{\bullet+}$, $\mathbf{9}^{2+}$, and $\mathbf{11}^{\bullet+}$ species, the absorption bands in the range 7700−9800 cm^{-1} and the deduced values of the reorganization energy λ, calculated by combining the experimentally determined ν_{max} with the electrochemical estimate of $\Delta G°$ ($\lambda = \nu_{max} - \Delta G°$) in the range of 6000−9800 cm^{-1}, are consistent with the assignment of the low-energy features of the present compounds as Fe(II)-to-Fe(III) IVCT bands.[2]

For the unsymmetrical mixed-valence ion $\mathbf{5}^{\bullet+}$, the comparison between $\Delta\nu_{1/2\ exp}$ and $\Delta\nu_{1/2\ theo}$ of the IVCT appearing at $\lambda =$ 1296 nm, which is usually diagnostic for the classification of a mixed-valence species, indicates that the experimental value (2785 cm^{-1}) is less than that predicted (3737 cm^{-1}) for a Class II mixed-valence species. Because $V_{ab} \ll \lambda$, this mixed-valence system belongs to Class II of Robin and Day nomenclature, because localization *versus* delocalization is determined by the relative magnitudes of V_{ab} and λ, which are characteristic of the mixed-valence ground state. For $\mathbf{5}^{\bullet+}$ $2V_{ab}/\lambda = 0.04$, this system is localized in the ground state, although the IVCT band is unusually narrow. The origin of this discrepancy is not immediately clear, although differences between theoretical and experimental values of $\Delta\nu_{1/2}$ are not uncommon. They often arise from system nonidealities with respect to the model.[33] In addition, the value of the Γ parameter (0.25) also indicates that this mixed-valence compound is a weakly coupled class II system[32] (Figure 5).

A similar study carried out on the mixed-valence species $\mathbf{9}^{2+}$ indicates that the experimental half-bandwidth (3886 cm^{-1}) for the IVCT band, appearing at $\lambda = 1228$ nm in the NIR, and that calculated (3860 cm^{-1}), are quite similar as expected for a class II mixed-valence species. This result is also in agreement with the value calculated for the Γ parameter (0.006), typical for weakly coupled class II systems.

Thus, in both cases, the electronic coupling V_{ab} can be calculated by the above-mentioned Hush equation, in which d_{ab}, the adiabatic electron-transfer distances (9.175 Å for $\mathbf{5}^{\bullet+}$ and 9.198 Å for $\mathbf{9}^{2+}$), were assumed to be equal to the geometrical metal−metal-distances obtained from DFT calculations. As a consequence, the values of V_{ab} of 122 cm^{-1} for $\mathbf{5}^{\bullet+}$ and 201 cm^{-1} for $\mathbf{9}^{2+}$, and the delocalisation coefficient α (0.016 for

(29) Ceccon, A.; Santi, S.; Orian, L.; Bissello, A. *Coord. Chem. Rev.* **2004**, *248*, 683.
(30) (a) Barlow, S. *Inorg. Chem.* **2001**, *40*, 7047. (b) Santi, S.; Orian, L.; Durante, C.; Bisello,; Benetollo, F.; Crociani, L.; Ganis, P.; Ceccon, A. *Chem.−Eur. J.* **2007**, *13*, 1955.
(31) Brunschwig, B. S.; Creuts, C.; Sutin, N. *Chem. Soc. Rev.* **2002**, *31*, 168.
(32) Brunschwig, B. S.; Sutin, N. *Coord. Chem. Rev.* **1999**, *187*, 233.
(33) (a) Elliot, C. M.; Derr, D. L.; Matyushov, D. V.; Newton, M. D. *J. Am. Chem. Soc.* **1998**, *120*, 11714. (b) Curtis, J. C.; Meyer, T. J. *Inorg. Chem.* **1982**, *21*, 1562.

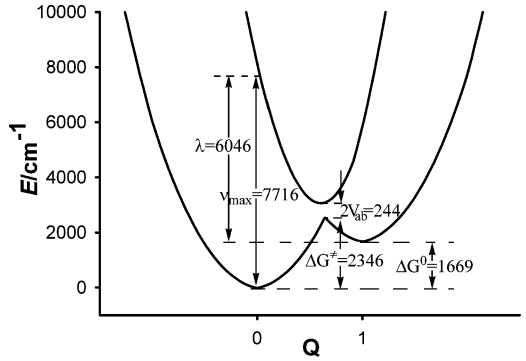

FIGURE 5. Potential energy curves and characteristic parameters for the MMCT band of mixed-valence $\mathbf{5}^{\bullet+}$.

$\mathbf{5}^{\bullet+}$ and 0.25 for $\mathbf{9}^{2+}$), are estimates only of the actual electronic coupling. Interestingly, for the mixed-valence compound $\mathbf{9}^{2+}$, the values of α and V_{ab} are of comparable magnitude to those found in 1,4-bis(ferrocenyl)-2-aza-1,3-butadiene[8] (α = 0.03; V_{ab} = 260 cm^{-1}).

Spectral deconvolution, assuming a Gaussian profile, and the application of the two-state Hush model to the band corresponding to the $Fe^{II}-Fe^{III}$ IVCT transition in the mixed-valence compound $\mathbf{11}^{\bullet+}$, and to the asymmetric $Ru^{II}-Fe^{III}$ IVCT transition in the dication $\mathbf{11}^{2+}$, reveals that the observed half-width ($\Delta\nu_{1/2\ exp}$ = 3356 and 2040 cm^{-1}) are markedly narrower than the half-width predicted ($\Delta\nu_{1/2\ theor}$ = 4744 and 3426 cm^{-1}). The MMCT study ($2V_{ab}/\lambda$: 0.03 for $\mathbf{11}^{\bullet+}$ and 0.07 for $\mathbf{11}^{2+}$), the large value of the comproportionation constant (K_c), the observation of a narrower bandwidth than predicted theoretically, and the resulting values of Γ = 0.30 for $\mathbf{11}^{\bullet+}$ and 0.40 for $\mathbf{11}^{2+}$ could suggest that these systems lie close to transition between Class II and Class II−III classification for a mixed-valence compound. Interestingly, the value of the electronic coupling parameter V_{ab}= 150 cm^{-1} calculated by deconvolution of the observed $Fe^{II}-Fe^{III}$ (18.617 Å) IVCT transition in the mixed-valence compound $\mathbf{11}^{\bullet+}$ indicates the ability of the ruthenocene system to promote a long distance intervalence electron-transfer.

Metal-Ion Sensing Properties. Metal recognition properties of the triads **5**−**12** were evaluated by electrochemical, optical, and ^1H NMR techniques. At first, the electrochemical behavior of these trimetallocene compounds was investigated in the presence of several metal cations such as Li^+, Na^+, K^+, Ca^{2+}, Mg^{2+}, Zn^{2+}, Cd^{2+}, Hg^{2+}, Ni^{2+}, and Pb^{2+} as their perchlorate salts.

One of the most interesting attributes of these ligands is the presence of differenciated redox-active metallocene moieties close to the cation-binding nitrogen atoms. Due to the absorption phenomena observed on the electrode's surface upon addition of metal cations, the electrochemical cation sensing experiments were carried out by using differential pulse voltammetry (DPV),[34] both in CH_2Cl_2 and CH_3CN solutions, containing [(*n*-Bu) $_4$N]PF_6 (0.1 M) as the supporting electrolyte. Remarkably, ligands **5**−**12** exhibited the same response upon the stepwise addition of Mg^{2+}, Zn^{2+}, Cd^{2+}, Hg^{2+}, Ni^{2+}, and Pb^{2+} metal ions in CH_2Cl_2 solutions. Thus, the titration studies with the addition of such set of metal perchlorate salts revealed a significant

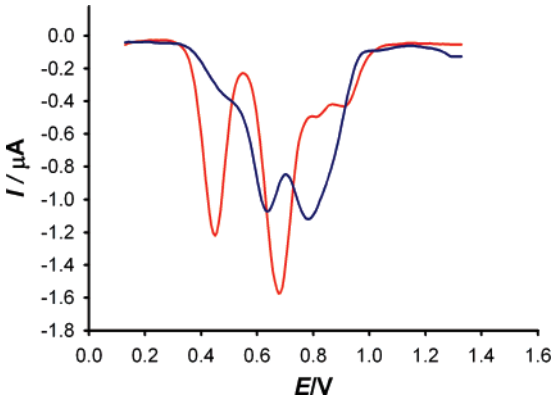

FIGURE 6. Evolution of the DPV of **5** (1 mM) in CH_2Cl_2 with [(*n*-Bu) $_4$N]PF_6 as supporting electrolyte scanned at 0.1 V s^{-1} from −0.7 to 1.4 V when 0 (red), and 1 equiv (blue) of Zn^{2+} are added.

perturbation of the two oxidation peaks, during the addition of 0−1 equiv of these metal cations. Therefore, a progressive decrease in the current intensity of both oxidation peaks were observed and simultaneously two new peaks appeared at more positive potentials, which were ascribed to the metal complexed species (Figure 6). It is worth mentioning that the height of the new peaks increases, reaching their maximun when 1 equiv of the metal cations was added; at this point, the two oxidation peaks of the free ligand disappear completely. In contrast, the addition of other metal ions (Li^+, Na^+, K^+, and Ca^{2+}) had no effect on their DPVs.

This cation selectivity changes markedly in CH_3CN solution. First of all, because of the very limited solubility of the trinuclear ligands **7**, **8**, **10**, and **12** in acetonitrile and the poor reversibility of their oxidation processes, the corresponding titration experiments could not be performed.

Thus, titration studies with addition of the above-mentioned set of metal cations to an electrochemical solution of receptor **5** ($c = 10^{-3}$ M) in CH_3CN demonstrate that whereas addition of Zn^{2+}, Hg^{2+}, and Pb^{2+} ions promotes remarkable responses, addition of Li^+, Na^+, K^+, Ca^{2+}, Mg^{2+}, Cd^{2+}, and Ni^{2+} metal ions had no effect on the DPV of this receptor, even when present in a large excess. In general, the results obtained on the stepwise addition of substoichiometric amounts of Zn^{2+}, Hg^{2+}, and Pb^{2+} revealed the appearance of two new peaks at more positive potential together with the two peaks corresponding to the free receptor (Table 4). The current intensity of these two new peaks increases until 1 equiv of the guest cations is added. At this point, the peaks corresponding to the uncomplexed receptor **5** disappear. The first oxidation peak of the free ligand, corresponding to the central ferrocene unit linked at the 4-position of the two bridges, shows a significant modification upon addition of these metal cations (ΔE_p = 200 mV). This particular behavior is characteristic of a large equilibrium constant for the binding of these cations by the neutral receptor.[35] Surprisingly, the second oxidation process of the complex $[\mathbf{5}^{\bullet}Me]^{2+}$, associated to the peripheral ferrocene units linked at the 1-position of the aza-bridges, was less perturbed on the addition of the guest cations (ΔE_p = 130 mV). This fact suggests that the complex starts to be disrupted after the first monoelectronic oxidation of that complex and then the second oxidation is taking place at a potential very close to that found for the uncomplexed mono-oxidized species $\mathbf{5}^+$.

(34) DPV technique has been employed to obtain well-resolved potential information, while the individual redox process are poorly resolved in the CV experiments in individual E1/2 potential can not be accurately extracted easily from this data. See: Serr, B. R.; Andersen, K. A.; Elliot, C. M.; Anderson, O. P. *Inorg. Chem.* **1988**, *27*, 4499.

(35) Miller, S. R.; Gustowski, D. A.; Chen, Z. H.; Gokel, G. W.; Echegoyen, L.; Kaifer, A. E. *Anal. Chem.* **1988**, *60*, 21021.

TABLE 4. Voltammetric and Complexation Data of Ligands 5, 9, and 11 in CH_3CN at 278 K

comp.	^1E_p[a]	^2E_p[b]
5	0.69	0.47
5·Zn^{2+}	0.82	0.67
5·Hg^{2+}	0.82	0.67
5·Pb^{2+}	0.82	0.67
9	0.51	0.84
9·Zn^{2+}	0.56	0.84
9·Hg^{2+}	0.61	0.84
9·Pb^{2+}	0.61	0.84
11	0.51	0.93
11·Zn^{+2}	0.56	0.93
11·Hg^{2+}	0.60	0.93
11·Pb^{2+}	0.60	0.93

[a] Oxidation potentials in V vs decamethylferrocene (DMFc) corresponding to the peripheral metallocene units. [b] Oxidation potentials in V vs DMFc corresponding to the central metallocene unit.

The structural differences of ligands **9** and **11** with respect to **5** are clearly demonstrated in their DPV responses. Although titration experiments, based on addition of the tested metal ions to a 10^{-3} M solution of ligands **9** and **11** in CH_3CN with [(*n*-Bu)$_4$N]PF_6,(0.1 M), showed binding affinities only for Zn^{2+}, Hg^{2+}, and Pb^{2+} metal ions, the electrochemical responses observed were completely different to those showed for receptor **5**. Stepwise addition of substoichiometric concentrations of these metal ions results in the appearance of a new two-electron oxidation peak shifted at a more positive potential corresponding to the simultaneous oxidation of the two peripheral ferrocene units. The current intensity of this new peak increases with the concentration of metal cations until 1 equiv is added; at this point, the original peak disappears and the new redox peaks reach full development, whereas the second one oxidation peak, corresponding to the oxidation of the central metallocene, is not perturbed during the addition of 1 equiv of Zn^{2+}, Hg^{2+}, or Pb^{2+}. This fact suggests that a full decomplexation of these divalent cations occurs during the electrochemical oxidation of the [**L**·Me]$^{4+}$ complex (**L** = **9** or **11** and Me = Zn^{2+}, Hg^{2+}, or Pb^{2+}), and then the third oxidation really takes place on the uncomplexed di-oxidized species **L**$^{2+}$. Similar features were observed when the electrochemical solution was treated with larger amounts of these metal cations.

Previous studies on ferrocene-based ligands have shown that their characteristic low-energy (LE) bands in the absorption spectra are perturbed upon complexation.[36] Therefore, the metal recognition properties of the aza-bridged metallocene triads **5**−**12** toward metal ions were also evaluated by UV−vis spectroscopy. Titration experiments for CH_2Cl_2 and CH_3CN solutions of ligand ($c = 1 \times 10^{-4}$ M) and the corresponding ions were performed and analyzed quantitatively.[37] No changes were observed in the UV−vis spectra upon addition of Li^+, Na^+, K^+, and Ca^{2+}, even in a large excess, to the CH_2Cl_2 solutions of any of these ligands. However, significant spectrophotometric changes in the LE absorption bands were observed upon addition of increasing amounts of Mg^{2+}, Zn^{2+}, Cd^{2+}, Hg^{2+}, Ni^{2+}, and Pb^{2+} metal ions. In all cases, the most prominent features observed during the complexation processes are the following: (1) a progressive red-shift of the corresponding LE band; (2) appearance of well defined isosbestic points, indicative of the presence of only two absorbing species in the solution the free ligand (**L**) and the complex (**L**.Me^{2+}); and (3) a neat change of the color during the complexation event, which is strongly affected by the position at which the metallocenes are linked to the aza-bridge, from orange to purple (for **5**−**8**), or to deep green (for **9**−**12**) and which can be used for the "naked eye" detection of these divalent cations. Analysis of the spectral titration data, using a computer program,[37] allowed us to determine the stoichiometry of the complexes as well as the binding constant (K_a) for the evaluated metal cations (see the Supporting Information).

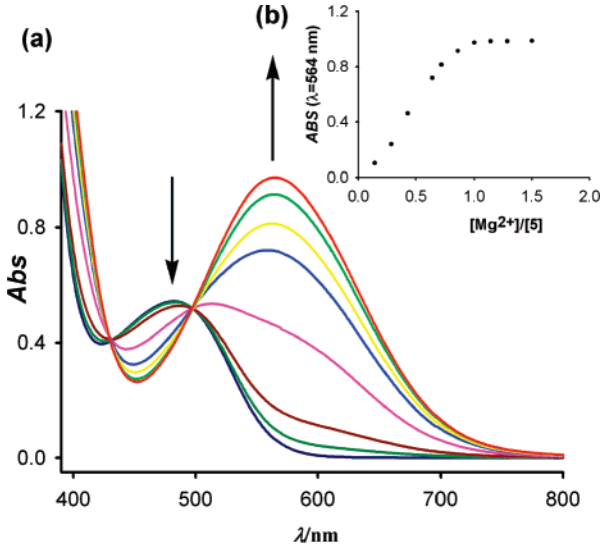

FIGURE 7. (a) Evolution of the UV−vis of **5**, upon addition of Mg^{2+}, arrows indicating the absorptions that increase or decrease during the titration experiment; (b) Changes of absorbance at 564 nm, upon addition of $Mg(ClO_4)_2$ to a CH_2Cl_2 solution of **5**.

As a representative case, the titration of the homotrimetallic ligand **5** with Mg^{2+} deserves some comments. The addition of increasing amounts of a solution of anhydrous $Mg(ClO_4)_2$ in CH_3CN ($c = 2.5 \times 10^{-2}$M) to a solution of **5** in CH_2Cl_2 ($c = 1 \times 10^{-4}$M) caused a progressive appearance of a new more intense band located at $\lambda = 564$ nm ($\epsilon = 9750$ M^{-1} cm^{-1}) as well as the complete disappearance of the initial LE band at $\lambda = 483$ nm ($\epsilon = 5190$ M^{-1} cm^{-1}) (Figure 7). Two well-defined isosbestic points at $\lambda = 428$ and 500 nm were found, indicating that a neat interconversion between the uncomplexed and complexed species occurs. The new band is red-shited by 81 nm and is responsible for the change of color from orange (neutral triad **5**) to deep purple (complexed triad **5**.Mg^{2+}). The resulting titration data suggest a 1:1 binding model (Figure 7b), the association constant being 1.02×10^6 M^{-1} (error < 10%).

Theoretical calculations show that the **5**·$Mg(ClO_4)_2$ complex should be formed upon rotation of one-half of the otherwise centrosymmetric most stable conformation of **5** and of one azadiene bridge, so as both nitrogen electron pairs point in a

(36) (a) Marder, S. R.; Perry, J. W.; Tiemann, B. G. *Organometallics* **1991**, *10*, 1896−1901. (b) Coe, B. J.; Jones, C. J.; McCleverty, J. A.; Bloor, D.; Cross, G. J. *J. Organomet. Chem.* **1994**, *464*, 225−232. (c) Müller, T. J.; Netz, A.; Ansorge, M. *Organometallics* **1999**, *18*, 5066−5074. (c) Carr, J. D.; Coles, S. J.; Asan, M. B.; Hurthouse4, M. B.; Malik, K. M. A.; Tucker, J. H. R. *J. Chem. Soc., Dalton Trans.* **1999**, 57.

(37) Specfit/32 Global Analysis System, 1999−2004 Spectrum Software Associates (SpecSoft@compuserve.com). The Specfit program was adquired from Bio-logic, SA (www.bio-logic.info) in January 2005. The equation to be adjusted by non-linear regression, using the above mentioned software was: $\Delta A/b = \{K_{11}\Delta\epsilon_{HG}[H]_{tot}[G]\}/\{1 + K_{11}[G]\}$, where H = host, G = guest, HG = complex, ΔA = variation in the absorption, b = cell width, K_{11} = association constant for a 1:1 model, and $\Delta\epsilon_{HG}$ = variation of molar absorptivity.

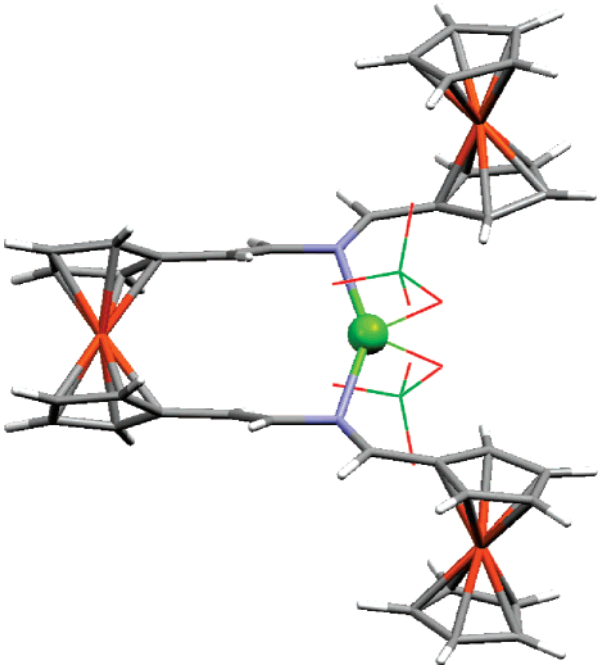

FIGURE 8. Calculated (B3LYP/6-31G*/Lanl2DZ-ecp) structure for the **5**·$Mg(ClO_4)_2$ complex (perchlorate ligands displayed in wireframe for clarity).

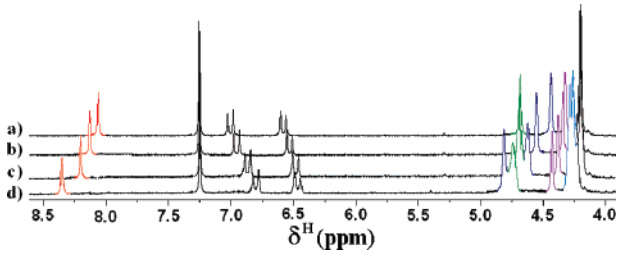

FIGURE 9. ^1H NMR spectrum of (a) free ligand **5** ($c = 1 \times 10^{-3}$ M) in $CDCl_3$ and upon addition of (b) 0.33, (c) 0.66, and (d) 1 equiv of Mg^{2+}.

convergent pincer-like fashion to the inner triferrocenic hinge cavity, to supply the two axial square-bipyramidal coordination positions around Mg^{2+} ion ($d_{N-Mg} = 2.238$ Å; $angle_{N-Mgn-N} = 138.9°$), the other equatorial positions being occupied by two different O atoms ($d_{O-Mg} = 2.129$ and 2.267 Å) of every perchlorate anion (Figure 8). For this complex, a high negative formation Gibbs free energy of −30.6 Kcal·mol^{-1} has been calculated in acetonitrile solution (see the Supporting Information).

To support the results obtained by UV−vis experiments, we also performed ^1H NMR titrations with the same set of metal cations. Thus, addition of 1 equiv of Mg^{2+} to a solution of the ligand **5** in $CDCl_3$ gives rise to significant downfield shifts for the signals corresponding to the iminic proton (C*H*═N) at $\delta = 8.07$ ppm ($\Delta\delta = +0.28$ ppm) as well as for the signals of the Cp protons appearing at $\delta = 4.69$ ($\Delta\delta = +0.12$ ppm) and at $\delta = 4.44$ ($\Delta\delta = +0.30$ ppm) together with a slight upfield shifs for the signals at $\delta = 6.99$ (C*H*═CH−N) ($\Delta\delta = -0.19$ ppm) and $\delta = 6.58$ (CH═C*H*−N) ($\Delta\delta = -0.11$ ppm) (Figure 9). These results are in agreement with above-mentioned calculated (B3LYP/6-31G*/Lanl2DZ-ecp) structure for **5**·$Mg(ClO_4)_2$, in which the nitrogen atoms within the azabutadiene bridges participate in the complexation process. Similar geometrical

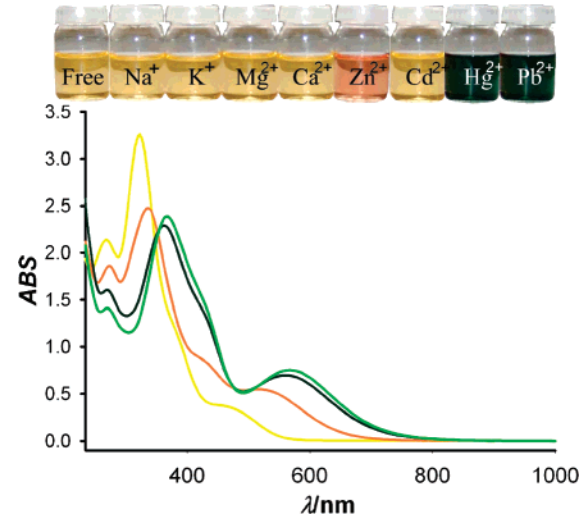

FIGURE 10. (Top) Changes in the color of the ligand **11** upon addition of several metal cations tested. (Bottom) Changes in the absorption spectra of compound **11** ($c = 10^{-4}$ M in CH_3CN) (yellow) upon addition of 1 equiv of Zn^{2+} (orange), Hg^{2+} (green), and Pb^{2+} (deep green).

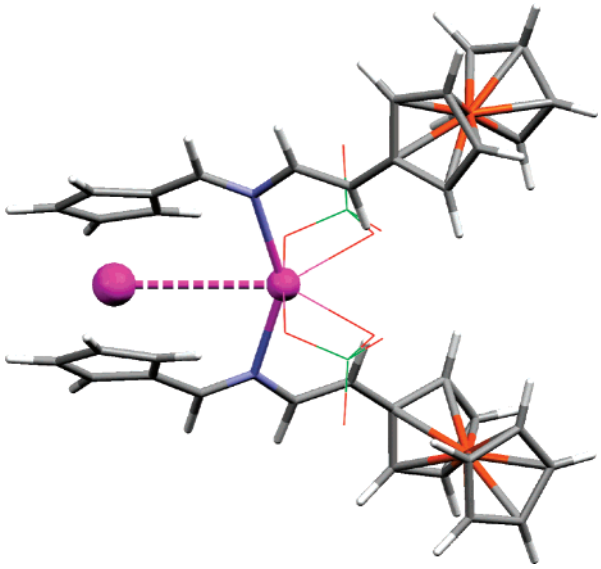

FIGURE 11. Calculated (B3LYP/6-31G*/Lanl2DZ-ecp) structure for the **11**·$Hg(ClO_4)_2$ complex (perchlorate ligands displayed in wireframe for clarity).

features were observed for the calculated structure of **5**·$Zn(ClO_4)_2$ (complexation $\Delta G°_{MeCN} = -42.6$ Kcal·mol^{-1}), as well as for the related complexes of the heterotrimetallic ligand **6** with $Mg(ClO_4)_2$ and $Zn(ClO_4)_2$ displaying similar complexation free energies ($\Delta G°_{MeCN} = -30.7$ and −41.9 Kcal·mol^{-1}, respectively) (see the Supporting Information).

In contrast to the above-mentioned results obtained in CH_2Cl_2 solutions, the complexation process of these ligands toward the same set of metal cations (Li^+, Na^+, K^+, Ca^{2+}, Mg^{2+}, Zn^{2+}, Cd^{2+}, Hg^{2+}, Ni^{2+}, and Pb^{2+}) in CH_3CN solutions revealed different selectivities to these specific analytes. Thus, whereas Li^+, Na^+, K^+, Ca^{2+}, Mg^{2+}, Cd^{2+}, and Ni^{2+} metal cations did not produce any detectable changes in the UV−vis spectra of such ligands, Zn^{2+}, Hg^{2+}, and Pb^{2+} induced the progressive appearance of a new LE band, red-shifted with respect to that observed in the free ligand, which in turn decreases continuously until disappearance when the total complexation is achieved.

TABLE 5. Relevant Physicochemical Data of the Free Ligand and Ligand/Metal Complexes Formed in CH_3CN

comp.		free	Zn^{2+}	Hg^{2+}	Pb^{2+}
5	λ^a	330 (26.26), 345 (sh), 480 (5.22)	351 (19.68), 556 (5.95)	351 (15.77), 556 (6.67)	351 (14.85), 556 (5.34)
	$\Delta\lambda^b$	-	76	76	76
	log K_{as}^c	-	5.1 ± 0.12	5.0 ± 0.11	5.3 ± 0.15
	L/M ^{d}	1/1	1/1	1/1	1/1
6	λ^a	332 (30.1), 460 (3.86)	366 (23.20), 551 (7.93)	366 (23.34), 551 (7.90)	366 (22.95), 551 (7.87)
	$\Delta\lambda^b$	-	91	91	91
	log K_{as}^c		4.8 ± 0.17	4.5 ± 0.12	4.8 ± 0.21
	L/M^d	1/1	1/1	1/1	1/1
9	λ^a	330 (30.20), 351 (sh), 462 (5.21)	335 (22.72), 367 (sh), 547 (3.6)	383 (22.49), 577 (7.50)	383 (22.56), 577 (7.41)
	$\Delta\lambda^b$	-	85	115	115
	log K_{as}^c		4.6 ± 0.10	5.3 ± 0.21	5.3 ± 0.18
	L/M^d	1/1	1/1	1/1	1/1
11	λ^a	321 (32.65), 454 (3.88)	337 (23.50), 417 (sh), 519 (5.51)	366 (23.94), 568 (7.58)	366 (22.98), 568 (6.98)
	$\Delta\lambda^b$	-	65	114	114
	log K_{as}^c		4.4 ± 0.17	5.2 ± 0.21	4.7 ± 0.15
	L/M^d	1/1	1/1	1/1	1/1

^{a} λ_{max}, in nm; ϵ, in $dm^3\ mol^{-1}cm^{-1}$. ^{b} Red-shift of the LE band upon metal complexation ($\Delta\lambda = \lambda_{complexed} - \lambda_{free}$). ^{c} Association constant determined by Specfit/32 Global Analysis System. ^{d} Stoichiometry of the complex formed (Ligand/Metal).

This solvent-dependent change of selectivity seems to be mainly originated by the important thermodynamic contribution of cations desolvation to the total complexation energy. At the working level of theory, we have found that in CH_3-CN the cavitation energy for the divalent metal ions increases in the following order $Hg^{2+} < Zn^{2+} < Ni^{2+} < Cd^{2+} < Mg^{2+}$ (2.82, 2.90, 3.00, 3.03, and 3.29 Kcal mol^{-1} respectively), whereas in CH_2Cl_2 the corresponding values are much lower (ranging from 2.46 to 2.86 Kcal mol^{-1}).

Addition of Zn^{2+}, Hg^{2+}, and Pb^{2+} metal cations to solution of the ligands **5** and **6**, in which the central metallocene is placed at 4-position of the aza-bridge, gives rise to the same red-shift of the corresponding LE band ($\Delta\lambda = 76$ and 91 nm, respectively), with simultaneous change in the color of the solution from orange to deep purple. However, the red-shift promoted for Hg^{2+} and Pb^{2+} metal cations upon addition to the ligands **9** and **11**, bearing the central metallocene linked to the 1-position of the aza-diene bridge, are of the same magnitude but different than that promoted by Zn^{2+}. Thus Hg^{2+} and Pb^{2+} metal cations promote a substancial change in the color of the solution from yellow to green, whereas Zn^{2+} metal cation induces a change from yellow to orange. In all cases, 1:1 binding models were also observed and the corresponding binding constants can also be determined by the analysis of the spectral titration data, by using the above-mentioned software (Table 5). Because of the very limited solubility of ligands **7**, **8**, **10**, and **11** in acetonitrile, titration experiments with them could not be performed.

The homo- and heterotrimetallic ligands **9** and **11**, respectively, are representative cases of this behavior. Thus, addition of increasing amounts of Hg^{2+} and Pb^{2+} to a solution of **9** and **11** in CH_3CN induced a red-shift of the LE bands from 462 ($\epsilon = 5.21\ M^{-1}\ cm^{-1}$) and 454 nm ($\epsilon = 3.88\ M^{-1}\ cm^{-1}$) to 577 ($\epsilon = 7.45\ M^{-1}\ cm^{-1}$) and 568 nm ($\epsilon = 7.53\ M^{-1}\ cm^{-1}$), respectively ($\Delta\lambda = 115$ and 114 nm, respectively). Simultaneously, the CH_3CN solutions change color from yellow to green, which can be used for "naked-eye" detection of Hg^{2+} and Pb^{2+} metal ions. In contrast, upon addition of Zn^{2+}, the LE bands present in the free ligands **9** and **11** also entirely disappeared and were replaced by a new band at $\lambda_{max} = 547$ ($\epsilon = 3.6\ M^{-1}\ cm^{-1}$) and 519 nm ($\epsilon = 5.51\ M^{-1}\ cm^{-1}$), respectively ($\Delta\lambda = 85$ and 65 nm, respectively). Furthermore, a simultaneous change of color in the solution, from yellow to orange, was also observed (Figure 9). In all these cases where an optical response could be detected, the observation of isosbestic points in the evolution of their UV−vis spectra clearly indicates that clean complexation equilibria take place. The association constants of the corresponding **9**·M^{2+} and **11**·M^{2+} (M = Zn^{2+}, Hg^{2+}, and Pb^{2+}) complexes formed could be evaluated by means of UV−vis spectrophotometric titration,[26] which also revealed a 1:1 stoichiometry for them. Although neither **9** nor **11** is particularly selective for the binding of one of these cations over the others, the difference in the change of colors promoted in the binding process is significant and, as a consequence, these ligands can be used for the selective colorimetric detection of Zn^{2+} or $Hg^{2+}$and Pb^{2+} (Figure 10).

For the reported constants to be taken with confidence, we have proved the reversibility of the complexation process by carrying out the following experiment: a stepwise addition of a solution of the receptor **11** in CH_3CN to a solution of the complex [**11**·Hg^{2+}] in the same solvent induced an increase of the absorption bands in the optical spectrum of the receptor, which is proportional to the amount of receptor added. This fact can be taken as clear evidence for reversibility. Moreover, extraction experiments also confirmed the high degree of reversibility of the complexation/decomplexation process: an equimolecular amount of $Hg(ClO_4)_2$ was added to a solution of **11** in CH_2Cl_2 to obtain the complexed [**11**·Hg^{2+}] species, whose DPV voltammogram and UV−vis spectrum were recorded. This solution was washed several times with water until the color of the solution changed from deep green to orange. The organic layer was dried, and the optical spectrum, DPV voltammogram, and ^1H NMR spectrum were recorded, and they were to be the same as that of the free receptor **11**. Afterward, an equimolecular amount of $Hg(ClO_4)_2$ was added to this solution and the initial UV−vis spectrum, DPV voltammogram, and ^1H NMR spectrum of the complex [**11**·Hg^{2+}] were fully recovered together with the deep green color. This experiment was carried out over several cycles, recording the optical spectrum after each step, and was fully recovered on complexation of the step.

Calculated structures for complexes **11**·$M(ClO_4)_2$ have been obtained for the divalent metal cations Mg^{2+}, Zn^{2+}, and Hg^{2+} as representative cases for different colorimetric behavior. They all show very similar geometrical features (Table 6) with mainly the expected small differences arising from the cation size ($Zn^{2+} < Mg^{2+} < Hg^{2+}$). The most significative difference is the rather short obtained Ru···Hg distance (3.825 Å), when compared to that of Mg or Zn, which is indicative of a not negligible Ru···Hg interaction (WBI_{Ru-Hg} 0.019) (Figure 11). Time dependent

TABLE 6. Selected Geometrical (Distances in Å, Angles in Degrees), Interaction, and TD−DFT Parameters for 11·M(ClO$_4$)$_2$ Complexes

	free	Mg^{2+}	Zn^{2+}	Hg^{2+}
d_{N-M}		2.280	2.201	2.427
(WBI) [a]		(0.069)	(0.127)	(0.173)
d_{O-M}		2.184	2.268	2.542
(WBI) [a]		(0.047)	(0.063)	(0.066)
		2.218	2.303	2.561
		(0.045)	(0.061)	(0.063)
d_{Ru-M}		4.148	4.066	3.825
(WBI)[a]		(0.003)	(0.005)	(0.019)
N−M−N		137.1	140.6	148.1
λ_{max} [b]	540.8	564.2	577.5	606.9
(*f*)[c]	0.035	(0.030)	(0.029)	(0.041)
Assignment	$Fe^{II}(d) \rightarrow \pi^*$	$Fe^{II}(d) \rightarrow \pi^*$	$Fe^{II}(d) \rightarrow \pi^*$	$Fe^{II}(d) \rightarrow Hg^{II}(s)$ $Fe^{II}(d) \rightarrow \pi^*$

[a] Wiberg bond index. [b] Unscaled (nm). [c] Oscillator strength (au).

DFT (TD−DFT) calculations revealed the occurrence of LE transitions (Table 6, only intense − *i.e.* with high oscillator strength − lowest-energy bands are collected) in agreement with the expected wavelength order as observed experimentally. The LE band responsible for the deep purple color in **11**·Hg(ClO$_4$)$_2$ can be adscribed to a Fe^{II}-to-Hg^{II} MMCT process. In sharp contrast, the corresponding LE bands in the analogous complexes of Mg^{2+} and Zn^{2+}, as well as in the free ligand **11**, correspond to MLCT processes, mainly from a $d_{x^2-y^2}$-type AO centered at both terminal Fe atoms, to an antibonding combination of the azadienes π^* MO with a d_{xz} or d_{yz}-type AO at the central Ru atom. The calculated complexation Gibbs free energies in solution ($\Delta G°_{MeCN} = -22.1$, -31.8, and -18.8 Kcal mol^{-1} for Mg^{2+}, Zn^{2+}, and Hg^{2+}, respectively) are lower than those obtained for the corresponding Mg^{2+} and Zn^{2+} complexes of **5** and **6**, their similarities accounting for the observed lack of selectivity.

Conclusion

The synthesis, electrochemical, and optical properties of homo- (**5**, **8**, **9**, and **12**) and heterometallic (**6**, **7**, **10**, and **11**) ferrocene-ruthenocene triads, are presented. These metallocenyl triads comprise remarkable multifunctional molecular systems, since they could serve as important models for the investigation of intramolecular electron transfer and for metal recognition processes. Triferrocenyl derivatives **5** and **9** form the mixed-valence species $\mathbf{5}^{\bullet+}$ and $\mathbf{9}^{2+}$ by partial oxidation, which shows intramolecular electro-transfer phenomena. Spectroelectrochemical studies of compound **11**, bearing two peripheral ferrocene units and one central ruthenocene moiety, revealed the presence of low-energy bands in the near-infrared (NIR) region, which indicate a rather unusual intramolecular charge-transfer between the ferrocene and ruthenocene units. Interestingly, the value of the electronic coupling parameter V_{ab}= 150 cm^{-1} calculated by deconvolution of the observed Fe(II)−Fe(III) IVCT transition in the mixed-valence compound $\mathbf{11}^{\bullet+}$, ($d_{Fe(II)-Fe(III)}$ = 18.617 Å), indicates the ability of the ruthenocene system to promote a long-distance intervalence electron-transfer.

On the other hand, the compounds studied exhibit interesting cation-sensing properties that show high selectivity for divalent metal cations giving response through two channels. Triads **5**, **9**, and **11** behave as dual redox and optical chemosensors for Zn^{2+}, Hg^{2+}, and Pb^{2+}. Their oxidation redox peaks are anodically shifted (up to 130 mV), and their low-energy (LE) bands of the absorption spectra are red-shifted (up to 115 nm) upon complexation with these metal cations. These changes in the absorption spectra are accompanied by dramatic color changes that allow the potential for "naked eye" detection. Compound **5** also exhibited a selective Hg^{2+} redox-induced complexation/decomplexation type of signaling pattern that can be used for the construction of more elaborate supramolecular switching systems.

Experimental Section

General Procedure for the Preparation of Homo- and Heterotrimetallocenes 5, 6, 7, and 8. To a solution of the appropriate diethyl [(metallocenylmethylidene)aminomethyl]-phosphonate **1** or **2** (3.3 mmol) in dry THF (15 mL), at −78 °C and under nitrogen atmosphere, *n*-BuLi 1.6 M in hexane (1.10 mL) was added. Then, a solution of the appropriate 1,1′-diformyl metallocene (1.65 mmol) in dry THF (10 mL) was slowly added, and the mixture was stirred for 1.5 h. The reaction mixture was allowed to reach the room temperature (30 min), and then it was heated under reflux temperature overnight. After the solution was cooled at 0 °C for 30 min, a precipitate was formed, which was filtered and washed with diethyl ether (2 × 10 mL) to give the corresponding trimetallocene, which was recrystallized from THF.

1,1′-Bis(2-aza-1-ferrocenyl-1,3-butadien-4-yl)ferrocene 5: 92%; mp > 350 °C. ^{1}H NMR (300 MHz, $CDCl_3$): δ 4.20 (s, 10H), 4.33 (st, 4H), 4.40 (st, 4H), 4.44 (st, 4H), 4.69 (st, 4H), 6.58 (d, 2H, J = 14.0 Hz), 6.99 (d, 2H, J = 14.0 Hz), 8.07 (s, 2H). ^{13}C NMR (75 MHz, $CDCl_3$): δ 68.2 (4CH), 68.9 (4CH), 69.3 (4CH), 69.7 (10CH), 70.3 (4CH), 71.0 (4CH), 80.9 (q), 82.9 (q), 125.7, 140.8, 158.9. MS (70 eV, EI): *m*/*z* (relative intensity): 660 (M^+, 100), 423 (50), 358 (98), 330 (34), 121 (46). Anal. Calcd for $C_{36}H_{32}Fe_3N_2$: C, 65.49; H, 4.89; N, 4.24. Found: C, 65.33; H, 5.04; N, 3.99.

1,1′-Bis(2-aza-1-ferrocenyl-1,3-butadien-4-yl)ruthenocene 6: 90%; mp = 250−254 °C (d). ^{1}H NMR (300 MHz, $CDCl_3$): δ 4.20 (s, 10H), 4.42 (st, 4H), 4.61 (st, 4H), 4.66 (st, 4H), 4.77 (st, 4H), 6.44 (d, 2H, J = 13.0 Hz), 6.94 (d, 2H, J = 13.0 Hz), 8.02 (s, 2H). ^{13}C NMR (75 MHz, $CDCl_3$): δ 68.7 (4CH), 69.2 (4CH), 69.3 (4CH), 71.1 (10CH), 71.2 (4CH), 81.3 (q), 86.3 (q), 125.4, 140.5, 160.2. FAB MS *m*/*z* (relative intensity): 706 (M^+ + 1, 100). Anal. Calcd for $C_{36}H_{32}Fe_2N_2Ru$: C, 61.30; H, 4.57; N, 3.97. Found: C, 61.53; H, 4.65; N, 3.71.

1,1′-Bis(2-aza-1-ruthenocenyl-1,3-butadien-4-yl)ferrocene 7: 82%; mp = 248−253 °C (d). ^{1}H NMR (300 MHz, $CDCl_3$): δ 4.25 (st, 4H), 4.30 (st, 4H), 4.60 (s, 10H), 4.75 (st, 4H), 5.06 (st, 4H), 6.52 (d, 2H, J = 13.0 Hz), 6.92 (d, 2H, J = 13.0 Hz), 7.93 (s, 2H). ^{13}C NMR (75 MHz, $CDCl_3$): δ 68.2 (4CH), 70.2 (4CH), 70.5 (4CH), 71.4 (10CH), 72.3 (4H), 82.6 (q), 85.3 (q), 125.7, 140.4, 158.2. FAB MS *m*/*z* (relative intensity): 751 (M^+ + 1, 100). Anal. Calcd for $C_{36}H_{32}FeN_2Ru_2$: C, 57.60; H, 4.30; N, 3.73. Found: C, 57.89; H, 4.55; N, 3.90.

1,1′-Bis(2-aza-1-ruthenocenyl-1,3-butadien-4-yl)ruthenocene 8: 87%; mp = 252−255 °C (d). ^{1}H NMR (200 MHz, $CDCl_3$): δ 4.58 (s, 10H), 4.60 (st, 4H), 4.70−4.73 (m, 8H), 5.01 (st, 4H), 6.35 (d, 2H, J = 13.0 Hz), 6.83 (d, 2H, J = 13.0 Hz), 7.87 (s, 2H). ^{13}C NMR (50 MHz, $CDCl_3$): δ 70.4 (4CH), 70.6 (10CH), 72.3 (4CH), 73.0 (4CH), 73.1 (4CH), 85.3 (q), 85.7 (q), 126.0, 140.3, 158.1. FAB MS *m*/*z* (relative intensity): 796 (M^+ + 1, 100). Anal. Calcd for $C_{36}H_{32}N_2Ru_3$: C, 54.33; H, 4.05; N, 3.52. Found: C, 54.59; H, 3.88; N, 4.27.

General Procedure for the Preparation of Homo- and Heterotrimetallocenes 9, 10, 11 and 12. To a solution of the appropriate 1,1′-metallocenediyl-bis(methylidenaminomethylphosphonate) **3** or **4** (1.65 mmol) in dry THF (15 mL), at −78 °C and under nitrogen atmosphere, *n*-BuLi 1.6 M in hexane (1.10 mL) was added. Then, a solution of the appropriate 1-formyl metallocene (3.3 mmol) in dry THF (10 mL) was slowly added, and the mixture was stirred for 1.5 h. The reaction mixture was allowed to reach

the room temperature (30 min), and then it was heated under reflux temperature overnight. After the solution was cooled at 0 °C for 30 min, a precipitate was formed, which was filtered and washed with diethyl ether (2 × 10 mL) to give the corresponding trimetallocene, which was recrystallized from THF.

1,1′-Bis(2-aza-4-ferrocenyl-1,3-butadien-1-yl)ferrocene 9: 90%; mp > 350 °C. ^{1}H NMR (200 MHz, $CDCl_3$): δ 4.14 (s, 10H), 4.27 (st, 4H), 4.37 (st, 4H), 4.45 (st, 4H), 4.79 (st, 4H), 6.65 (d, 2H, J = 14.0 Hz), 7.00 (d, 2H, J = 14.0 Hz), 7.97 (s, 2H). ^{13C} NMR (50 MH_z, $CDCl_3$): δ 67.1 (4CH), 69.2 (10CH), 69.4 (4CH), 69.7 (4CH), 72.1 (4CH), 73.3 (4CH), 81.9 (q), 82.2 (q), 127.4, 140.3, 159.2. MS (70 eV, EI): *m*/*z* (relative intensity): 660 (M^+, 100), 595 (30), 476 (30), 358 (70), 330 (43), 130 (46). Anal. Calcd for $C_{36}H_{32}Fe_3N_2$: C, 65.49; H, 4.89; N, 4.24. Found: C, 65.28; H, 5.16; N, 4.21.

1,1′-Bis(2-aza-4-ruthenocenyl-1,3-butadien-1-yl)ruthenocene 10: 81%; mp = 250−253 °C (d). ^{1}H NMR (200 MHz, $CDCl_3$): δ 4.43 (st, 4H), 4.54 (s, 10H), 4.61 (st, 4H), 4.78 (st, 4H), 4.82 (st, 4H), 6.52 (d, 2H, J = 13.0 Hz), 6.95 (d, 2H, J = 13.0 Hz), 7.91 (s, 2H). ^{13}C NMR (50 MHz, $CDCl_3$): δ 68.0 (4CH), 70.1 (4CH), 71.3 (10CH), 71.4 (4CH), 72.5 (4CH), 82.3 (q), 85.1 (q), 125.8, 140.2, 158.3. FAB MS *m*/*z* (relative intensity): 751 (M^+ + 1, 100). Anal. Calcd for $C_{36}H_{32}FeN_2Ru_2$: C, 57.60; H, 4.30; N, 3.73. Found: C, 57.35; H, 4.41; N, 4.02.

1,1′-Bis(2-aza-4-ferrocenyl-1,3-butadien-1-yl)ruthenocene 11: 92%; mp = 251−255 °C (d). ^{1}H NMR (400 MHz, $CDCl_3$): δ 4.13 (s, 10H), 4.24 (st, 4H), 4.33 (st, 4H), 4.77 (st, 4H), 5.13 (st, 4H), 6.57 (d, 2H, J = 13.0 Hz), 6.90 (d, 2H, J = 13.0 Hz), 7.80 (s, 2H). ^{13}C NMR (100 MHz, $CDCl_3$): δ 67.0 (4CH), 69.0 (4CH), 69.2 (10CH), 71,6 (4CH), 73.5 (4CH), 81,7 (q), 86.5 (q), 127.3, 139.8, 157.2. FAB MS *m*/*z* (relative intensity): 706 (M^+ + 1, 100). Anal. Calcd for $C_{36}H_{32}Fe_2N_2Ru$: C, 61.30; H, 4.57; N, 3.97. Found: C, 61.08; H, 4.45; N, 4.26.

1,1′-Bis(2-aza-4-ruthenocenyl-1,3-butadien-1-yl)ruthenocene 12: 72%; mp = 249−251 °C (d). ^{1}H NMR (200 MHz, $CDCl_3$): δ 4.49 (s, 10H), 4.59 (st, 4H), 4.74 (st, 4H), 4.78 (st, 4H), 5.05 (st, 4H), 6.45 (d, 2H, J = 13.0 Hz), 6.84 (d, 2H, J = 13.0 Hz), 7.73 (s, 2H). ^{13}C NMR (50 MHz, $CDCl_3$): δ 70.4 (4CH), 70.5 (4CH), 71,0 (10CH), 72.4 (4CH), 72.6 (4CH), 85.3 (q), 85.8 (q), 125.3 141.0, 158.3. MS (70 eV, EI): *m*/*z* (relative intensity): 795 (M^+, 10), 526 (30), 245 (50), 167 (100). Anal. Calcd for $C_{36}H_{32}N_2Ru_3$: C, 54.33; H, 4.05; N, 3.52. Found: C, 54.57; H, 3.31; N, 3.24.

Preparation of 1,1′-Bis(2-aza-1-*p*-methoxyphenyl-1,3-butadien-4-yl)ferrocene 15. This compound was prepared following the general procedure previously described for the preparation of trimetallocenes **5**−**6**, but using *p*-methoxybenzaldehyde in the second step of the synthetic sequence. 60%; mp = 148−149 °C. ^{1}H NMR (300 MHz, $CDCl_3$): δ 3.86 (s, 6H), 4.29 (st, 4H), 4.37 (st, 4H), 6.62 (d, 2H, J = 13.2 Hz), 6.86 (d, 4H, J = 8.7 Hz), 7.06 (d, 2H, J = 13.2 Hz), 7.60 (d, 4H, J = 8.7 Hz), 8.05 (s, 2H). ^{13}C NMR (75 MHz, $CDCl_3$): δ 55.3, 68.3, 70.2, 82.6 (q), 114, 127, 129.3 (q), 129.8, 140.4, 158.2, 161.5 (q). FAB MS *m*/*z* (relative intensity): 505 (M^+ + 1, 100). Anal. Calcd for $C_{30}H_{28}FeN_2O_2$: C, 71.44; H, 5.60; N, 5.55. Found: C, 71.20; H, 5.88; N, 5.79.

Preparation of 1,1′-Bis(2-aza-4-*p*-methoxyphenyl-1,3-butadien-1-yl)ferrocene 16. This compound was prepared following the general procedure previously described for the preparation of trimetallocenes **9**−**10**, but using *p*-methoxybenzaldehyde in the second step of the synthetic sequence. 85%; mp = 139−140 °C. ^{1}H NMR (300 MHz, $CDCl_3$): δ 3.80 (s, 6H), 4.45 (st, 4H), 4.84 (st, 4H), 6.73 (d, 4H, J = 8.0 Hz), 6.80 (d, 2H, J = 14.0 Hz), 7.26−7.20 (m, 6H), 8.00 (s, 2H). ^{13}C NMR (75 MHz, $CDCl_3$): δ 69.7, 71.7, 71.9, 82.0 (q), 114, 127.6, 129.3 (q), 129.8, 149.9, 159.0, 160.7 (q). FAB MS *m*/*z* (relative intensity): 505 (M^+ + 1, 100). Anal. Calcd for $C_{30}H_{28}FeN_2O_2$: C, 71.44; H, 5.60; N, 5.55. Found: C, 71.19; H, 5.35; N, 5.69.

Preparation of 1,1′-Bis(2-aza-4-*p*-methoxyphenyl-1,3-butadien-1-yl)ruthenocene 17. This compound was prepared following the general procedure previously described for the preparation of trimetallocenes **11**−**12**, but using *p*-methoxybenzaldehyde in the second step of the synthetic sequence. 87%; mp = 165−166 °C. ^{1}H NMR (300 MHz, $CDCl_3$): δ 3.77 (s, 6H), 4.75 (st, 4H), 5.14 (st, 4H), 6.68 (d, 4H, J = 8.0 Hz), 6.71 (d, 2H, J = 13.0 Hz), 7.10 (d, 2H, J = 13.0 Hz), 7.17 (d, 4H, J = 8.0 Hz), 7.80 (s, 1H). ^{13}C NMR (75 MHz, $CDCl_3$): δ 55.1, 71.7, 73.4, 86.3 (q), 113.9, 127.5, 128.3, 128.8 (q), 140.6, 158.5, 158.9 (q). EI MS *m*/*z* (relative intensity): 550 (M^+, 40), 402 (100), 160 (70). Anal. Calcd for $C_{30}H_{28}N_2O_2Ru$: C, 65.56; H, 5.13; N, 5.10. Found: C, 65.30; H, 4.98; N, 5.32.

Acknowledgment. We gratefully acknowledge a grant from MEC-Spain CTQ2004-02201 and from Fundación Séneca (CARM) 02970/PI/05. A.C. also thanks Ministerio de Educación y Ciencia for a predoctoral grant.

Supporting Information Available: NMR spectra. Electrochemical data of compounds **5**−**11**. Evolution of the UV−vis−NIR spectra during the course of the oxidation processes. Deconvolution of the NIR spectra. Relevant physicochemical data corresponding to the free and complexed ligands in CH_2Cl_2. Electrochemical data corresponding to the free and complexed ligands **5**, **9**, and **11** in CH_2Cl_2. Calculated structures, Cartesian coordinates and enegies. This material is available free of charge via the Internet at the http://pubs.acs.org.

JO071066G